BRNO UNIVERSITY OF TECHNOLOGY
VYSOKÉ UČENÍ TECHNICKÉ V BRNĚ

FACULTY OF MECHANICAL ENGINEERING
FAKULTA STROJNÍHO INŽENÝRSTVÍ

INSTITUTE OF MATERIALS SCIENCE AND ENGINEERING
ÚSTAV MATERIÁLOVÝCH VĚD A INŽENÝRSTVÍ

COLD SINTERING: NEW OPPORTUNITIES FOR ADVANCED CERAMIC MATERIALS
NOVÉ MOŽNOSTI STUDENÉHO SLINOVÁNÍ U POKROČILÝCH KERAMICKÝCH MATERIÁLŮ

MASTER'S THESIS
DIPLOMOVÁ PRÁCE

AUTHOR — **Bc. Jakub Hladík**
AUTOR PRÁCE

SUPERVISOR — **doc. Ing. David Salamon, Ph.D.**
VEDOUCÍ PRÁCE

BRNO 2021

BRNO UNIVERSITY OF TECHNOLOGY
FACULTY OF MECHANICAL ENGINEERING

Assignment Master's Thesis

Institut:	Institute of Materials Science and Engineering
Student:	**Bc. Jakub Hladík**
Degree programm:	Applied Sciences in Engineering
Branch:	Materials Engineering
Supervisor:	**doc. Ing. David Salamon, Ph.D.**
Academic year:	2020/21

As provided for by the Act No. 111/98 Coll. on higher education institutions and the BUT Study and Examination Regulations, the director of the Institute hereby assigns the following topic of Master's Thesis:

Cold sintering: new opportunities for advanced ceramic materials

Brief Description:

Cold sintering is an unusually low–temperature process that uses a transient transport phase, which is most often liquid, and an applied uniaxial pressure to assist in the densification of a powder compact. Current observations in several systems suggest a multiple–stage densification process that bears similarity to models that describe liquid phase sintering. Regardless of unclear sintering mechanisms, these low temperatures create a new opportunity spectrum to design new types of composite and low energy–consuming processes.
The aim of this work is the literature review, to establish a simple cold sintering apparatus and run tests on ceramic oxide systems.

Master's Thesis goals:

1. Literature review on the topic "cold sintering".
2. Assistance in assembling of the cold sintering apparatus.
3. Testing of cold sintering equipment(s).
4. Analysis of opportunities in the cold sintering.

Recommended bibliography:

GUO J., A. L. BAKER, H. GUO, M. LANAGAN and C. A. RANDALL. Cold sintering process: A new era for ceramic packaging and microwave device development. Journal of the American Ceramic Society. 2017, 100 (2), 669-677.

LIU, Y., Q. SUN, D. WANG, K. ADAIR, J. LIANG and X. SUN. Development of the cold sintering process and its application in solid-state lithium batteries. Journal of Power Sources [online]. 2018, 393, 193-203 [cit. 2020-11-24]. ISSN 03787753. Dostupné z: doi:10.1016/j.jpowsour.2018.05.015

GUO, J., R. FLOYD, S. LOWUM, J. P. MARIA, T. HERISSON DE BEAUVOIR, J. H. SEO and C. A. RANDALL. Cold Sintering: Progress, Challenges, and Future Opportunities. Annual Review of Materials Research [online]. 2019, 49 (1), 275-295 [cit. 2020-11-24]. ISSN 1531-7331. Dostupné z: doi:10.1146/annurev-matsci-070218-010041

Deadline for submission Master's Thesis is given by the Schedule of the Academic year 2020/21

In Brno,

L. S.

prof. Ing. Ivo Dlouhý, CSc.
Director of the Institute

doc. Ing. Jaroslav Katolický, Ph.D.
FME dean

ABSTRACT

A Cold sintering process (CSP) is a novel densification technique. It is a dissolution/precipitation-based process where material diffusion is enhanced by a presence of a transient solvent. That and a uniaxial pressing allows sintering of ceramics and glasses at a very low temperature of < 300 °C. Important factors for the CSP are the appropriate combination of a transient liquid (solvent) and powder. Advantages of the method are the low processing temperatures which decrease energy and economic costs, but also the possibility to prepare new types of composites. The technology has also a potential to become a leading process for production of small ceramic electronic devices when the sintering condition of a required ceramic will be mastered. Because CSP would spare noble metals used for, their thermal stability.

In the experimental part double stage die was prepared for a high-pressure mode of sintering in SPS. The silicon carbide die (reinforced by a steel ring) was enclosed by graphite die to ensure both mechanical properties and electric and thermal conductivity. Thus, the prepared die was successfully used for cold sintering at a temperature of 300 °C and 350 MPa.

Prepared dies were tested in practice during a study of a cold sintering phenomenon. Various factor and their effect on densification were studied using an advance of a dilatometric device and a vacuumable chamber. The specific issues of sintering of a ZnO in acetic acid were discussed, such as an importance of a soaking time/reaction time, sealing and vapor escape, temperature, and pressure. Plus, preliminary attempts to sinter a barium titanate ceramic were made.

KEYWORDS

Low-temperature sintering, cold sintering process, sintering mechanism, ceramics, spark plasma sintering, high pressure, solvent

ABSTRAKT

Cold sintering process (CSP) je nová metoda pro slinování keramik a skel. Tato metoda vede ke snížení teploty (<300 °C) a doby potřebné ke slinování. CSP se vyznačuje přítomností přechodné fáze a jednoosým lisováním. Principiálně se jedná o rozpouštěcí/precipitační proces. Metoda umožňuje slinutí dnes již široké škály keramik při teplotách hluboko pod teplotou tání. Jako přední výhodou nízkoteplotního slinování se jeví možnost přípravy nových typů struktur a kompozitů. Použití CSP se nabízí v elektrotechnickém průmyslu, kde by jeho aplikace mohla vést ke snížení energetické náročnosti výroby, a ke snížení teplotní zátěže výrobních zařízení. CSP by mohlo do značné míry omezit používání ušlechtilých (a drahých) kovů při výrobě drobných elektrických keramických součástek (například kondenzátorů) kde je jejich použití vynuceno vysokými procesními teplotami.

Experimentální část práce je zaměřena na přípravu vysokotlaké lisovací formy pro slinování v zařízení SPS. Z principu funkce SPS a požadavků na funkci, musí být forma elektricky a tepelně vodivá a musí být dostatečně pevná, aby odolávala vnitřním tlakům. V diplomové práci je tento problém řešen použitím dvojdílné formy. Forma se skládá z velké (vnější) grafitové formy, která vede elektrický proud a zprostředkovává ohřev. V této formě je uzavřena menší forma, která vlivem rozdílného poloměru pístu zvyšuje tlak na vzorek. Vnitřní forma je vyrobena z karbidu křemíku předepjatého ocelovou výztuží. Rozraní mezi oběma formami je zajištěno vložkami z nitridu křemíku. Materiál vnitřní formy byl vybrán pro svou tvrdost, pevnost, chemickou odolnost a odolnost vůči teplotním šokům. Předepnutí bylo provedeno za tepla nalisovanou bezešvou ocelovou trubkou. V praktické části byla forma úspěšně použita pro slinování vzorků při tlaku 350 MPa a teplotách nad 300 °C. Avšak očekává se i vyšší odolnost do 500 MPa.

Dále byla studována metoda CSP, s využitím zařízení pro Spark Plasma Sintering (SPS). Přistupovalo se k vy-vakuovaní komory zařízení, aby bylo možné sledovat vývoj par během slinování. Teplota slinování byla kontrolována termočlánkem umístěném ve stěně vnější – grafitové – formy. Vysokotlaké slinování bylo doplněno o slinování při nízkém tlakovém režimu (50 MPa) v čistě grafitové formě. Práce se z velké části zabývá studiem vnitřních a vnějších faktorů ovlivňujících slinování oxidu zinečnatého. Mezi studované vnitřní faktory patří: chemické složení a množství rozpouštědla, postup přípravy směsi, doba reakce mezi rozpouštědlem a práškem a těsnost formy. Pro přípravu keramiky ZnO keramiky byli použity dva druhy rozpouštědla: demineralizovaná voda a 1 M roztok kyseliny octové. Množství roztoku se pohybovalo od 5 do 25 hm%. Pro přípravu směsi rozpouštědla byl prášek buď mechanicky smíchán v porcelánovém hmoždíři nebo byl suchý prášek předlisován a poté vlhčen. Vlčení předlisovaných peletek bylo prováděno dvěma způsoby: nakapáváním roztoku na povrch vzorku nebo samovolným vzlínáním kapaliny z navlhčeného substrátu. Dále byla připravené směsi poskytnuta doba pro proběhnutí chemické reakce a studován její vliv na slinutí. Posledním studovaným vnitřním faktorem byla těsnost lisovací formy a její vliv na únik páry během slinování. Těsnost formy se lišila už

samotným designem formy. Z důvodu přesnějších tolerancí vysokotlaká forma lépe bránila úniku plynu v porovnání s nízkotlakou grafitovou formou. Dále bylo možné těsnost formy zlepšit hliníkovým těsněním. V případě vnějších vlivů byl studován dopad slinovací teploty, rychlosti ohřevu, a aplikované zatížení na slinování.

Výhodou slinování v zařízení SPS byla přítomnost integrovaných měřících systémů pro zaznamenání dilatace a hloubky vakua. Získané vzorky byli hodnoceny na základě dosažené teoretické hustoty, která byla měřena Archimedovou metodou, ale byla také studovaná mikrostruktura vzorků pomocí rastrovací elektronové mikroskopie. Slinování oxidu zinečnatého v čisté vodě nebylo efektivní a maximální relativní hustota nepřesáhla 85 %, avšak i toto je významný posun oproti 51 % pokud nebyla použita žádná kapalina. Nicméně aplikací roztoku octanu hlinitého bylo možné dosáhnout vzorku s relativní hustotou až 99,5 % při teplotě slinování 300 °C.

Jako méně vhodným vlhčícím postupem se ukázalo vlhčení předlisovaných peletek. Protože při vzlínání a kapaní vodného roztoku docházelo nehomogenní distribuci kapaliny a následně k nestejnorodému slinutí. Standardní dvacetiprocentní hmotnostní podíl roztoku kyseliny octové ve směsi byl vhodný pro slinování v neizolované grafitové nízkotlaké (jedno-dílné) formě, avšak nepříliš vhodný pro slinování při vysokých tlacích vlivem častého úniku směsi způsobenou nízkou viskozitou prášku. Použití hliníkového těsnění, zabraňují úniku plynu ze slinovací formy, mělo spíše negativní vliv na proces slinování, především při vyšším obsahu kapalné složky. Únik kapaliny během je CSP důležitý, protože vede ke vzniku přesyceného roztoku a zároveň umožní úplné uzavření pórů. V práci byl potvrzen jednoznačně pozitivní vliv slinovací teploty na zhutnění. V případě rychlosti ohřevu však nebyl zaznamenán významný rozdíl mezi dosaženými výsledky. Použití vysokých tlaků nemělo velký přínos pro slinování ZnO, protože hutnou keramiku bylo možné připravit již při tlacích 50 MPa. Avšak slinovací zařízení bude moci být v budoucnosti použito pro slinování obtížněji slinovatelných keramik.

KLÍČOVÁ SLOVA

Nízko-teplotní slinování, proces studeného slinování, mechanismus slinování, keramika, spark plasma sintering, vysoký tlak, rozpouštědla

HLADÍK, Jakub. *Nové možnosti studeného slinování u pokročilých keramických materiálů* [online]. Brno, 2021 [cit. 2021-05-20]. Dostupné z: https://www.vutbr.cz/studenti/zav-prace/detail/132913. Diplomová práce. Vysoké učení technické v Brně, Fakulta strojního inženýrství, Ústav materiálových věd a inženýrství. Vedoucí práce David Salamon.

DECLARATION

I declare that this master's thesis: Cold sintering: new opportunities for advanced ceramic materials have been worked out on my own using literature that I cited according to the rules.

In Brno on the 23. 5. 2021

.....

Bc. Jakub Hladík

ACKNOWLEDGEMENTS

I would like to express my gratitude to my supervisor doc. Ing. David Salamon, Ph.D. for his help, extraordinarily professional and friendly approach, kindness, valuable advice, and recommendations and supervision. Furthermore, I would like to thank all workers in a research group of advanced ceramic materials in CEITEC for helping me with experiments for my master's and bachelor's thesis.

Also, I would like to express my thanks to my family for the unconditional support throughout my whole studies.

CONTENT

1 INTRODUCTION

Ceramics is the oldest artificial group of materials. The oldest known ceramic is the statuette of Venus, which was discovered in Dolní Věstonice. The statuette is believed to be 29,000–25,000 years old which makes it the oldest artifact ever find. In contrast, the oldest metal artifact discovered: cooper beads, pins, and awls are dated just back to an area 8,000 B.C. [1]

Although traditional pottery has an impressive history. The development of a technical ceramic started recently. Modern ceramics have a wide range of applications due to their strong covalent and ionic bond. The use of ceramic is generally limited by the costs of processing it. Because ceramics has a generally high melting point. Apart from glass and glass-ceramics, casting is insufficient or unavailable for this material category. Therefore, processing temperatures are reduced by sintering. Conventional sintering works at temperatures above half the melting temperature. Because the melting points of most technical ceramics excite two thousand degrees Celsius, these temperatures are still high.

Recent studies have shown that the processing temperatures can be reduced even further. The cold sintering process (CSP) is one of the approaches. The first who set the Cold sintering terminology was Randall et al. by their patent in 2016. The process is inspired by hydrothermal synthesis. Using CSP, some materials were prepared at temperatures reaching only twenty percent of the melting point. The low sintering temperature is advantageous not only for energy and cost-saving but also for new possibilities. With a CSP it is possible to combinate ceramics and metal or even a polymer in one step. Since the temperature might be decreased by a CSP it would be possible to directly process a composite without degrading the material with low thermal stability. [2]

The term “cold sintering” is not entirely new. It was first used by Gutmanas et al. 1978 in the work “Cold sintering under high pressure” [3]. However, this study does not work with any form of a sintering aid (transient liquid). Although the sintering was processed at an ambient temperature the mechanism is different from the topic of the thesis. The sintering mechanism was based on plastic flow. Metallic powders such as Al, Cu, Fe, Co, oxides, or salts have been sintered by extremely high pressure (up to 10 GPa) [4].

2 GOALS OF THE WORK

The aims of this master's thesis are:

- Literature review on the topic "cold sintering".
- Assistance in assembling of the cold sintering apparatus.
- Testing of cold sintering equipments.
- Analysis of opportunities in the cold sintering.

3 THEORETICAL PART

3.1 Conventional sintering techniques

Forming

The task of a forming is to consolidate ceramic powder into a compact "green body". The shape of a body should be similar to a final product to minimize machining. The shaping techniques should ideally produce green bodies with a homogenous structure and with a minimal defect size. There are many groups of forming methods: wet forming (slip casting, gel casting, etc.), dry methods (uniaxial pressing, isostatic pressing, etc), plastic shaping (injection molding, extrusion, etc.).

3.1.1 Solid-phase sintering

The sintering is densification thermally activated process led by diffusion. The temperature of sintering is below the melting point. Driving force is related to a pressure gradient at the surface according to $\Delta P = \frac{2\gamma}{R}$. Where γ is the surface energy between solid and gas and R is a radius of a particle.

Solid-phase sintering is characteristic with a temperature of sintering below a melting point of material. It is one of the pressureless techniques, so it does not require an expensive die and it can be grafted with almost any forming method. The principle is usually described by three stages which are described by a character of porosity.

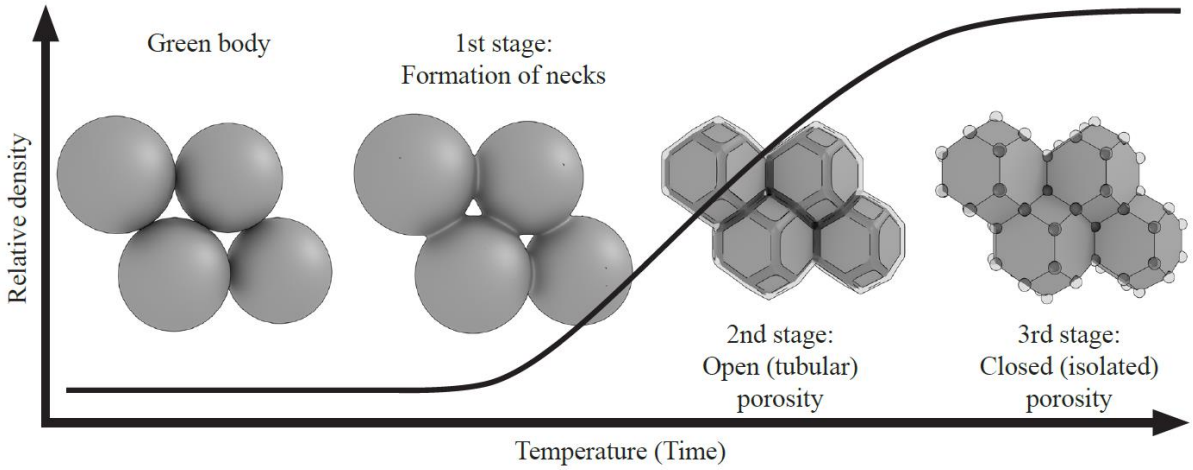

Figure 1 Stages of sintering, from: [5]

The first stage is associated with a neck formation at contact points of grain sides. The material transport is intermediated by diffusion, vapor transport, and plastic or viscous flow. Mechanism of the neck growth is assumed to last till the moment when the neck reaches 40–50 % size of particle radius.

The necking leads to an increase in mechanical properties and a shrinkage of a ceramic body (3–5 %) [6].

The second stage of sintering is distinguished by the existence of open porosity. The growth of necks results in a formation of a continuous network of channels. Surface tension leads to a further decrease of an area making the channels cross-section thinner. As a result, the ratio of diameter and length of the network decreases. During the second phase of sintering, the rate of shrinking is the biggest as visible in the Figure 1. Depending on the initial compaction of a powder, the second phase takes place in an interval from 50 to 90 %TD. At the final, the channel network is unstable, channels deflate, forming isolated pores [5].

The third and final stage begins when the open porosity is transformed onto a closed one. Generally, the microstructure evolution is described as a transformation of ideally round particles on polygonal grains. Hence, open porosity would appear at interstitial sites of an initial structure.

The total energy of the system might be reduced by a coarsening of particles and by densification which leads replaces of a solid/gas by interface by a solid/solid boundary. Both phenomena take place during sintering. Generally, there is an effort to suppress coarsening effect because of the energy efficiency and mechanical properties.

3.1.2 Thermodynamic of a sintering

Two pathways lead to a decrease in surface energy a) the coarsening of particles, b) the sintering (Both examples are visualized in the Figure 2). The coarsening leads to a decrease of a surface/volume ratio, reducing a total area of a gas/solid interface. Therefore, the total energy is also decreased.

In the case of sintering, the total energy is reduced by replacing of gas/solid interface with a solid/solid interface that has lower surface energy. According to these effects, total energy can be described by an equation:

$$\Delta(\gamma^{SG}A) = (\gamma^{SG} - \gamma^{SS})A + \gamma^{SG}\Delta A \qquad (1)$$

Where γ^{SG} is the surface energy of solid/gas interface, A is the initial surface area of powder, $(\gamma^{SG} - \gamma^{SS})$ is the change of interfacial energy due to a formation of a grain boundary, γ^{SS} is the surface energy of a solid/solid interface and ΔA is a gange of the surface due to a coarsening.

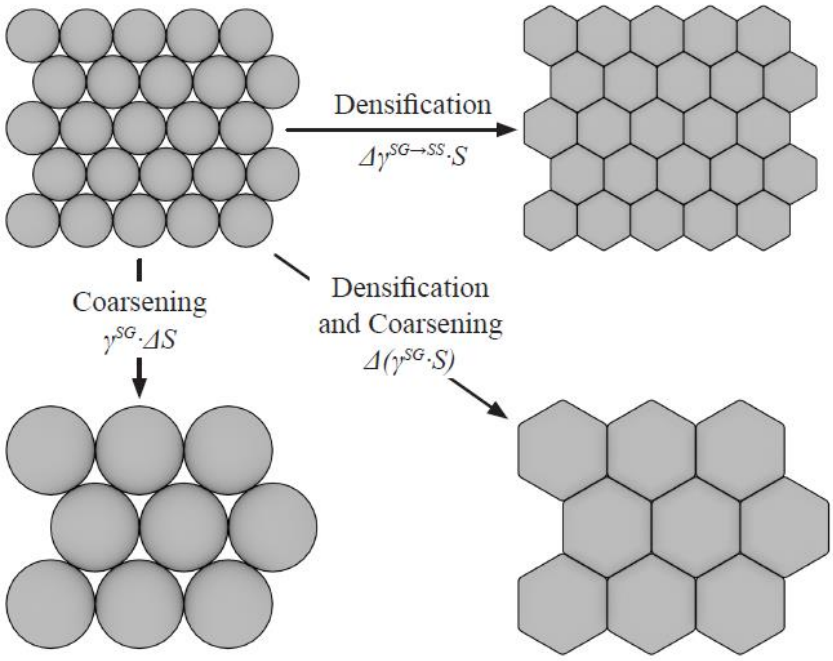

Figure 2 An illustration of a coarsening and densification, from: [5]

In Equation 1 both members (representing the coarsening and densification) have a negative value, so they always take place. Coarsening however is less desirable since it has often an adverse effect on some mechanical properties. [5]

3.1.3 Liquid phase sintering

Liquid phase sintering (LSP) runs in a presence of melted reactant. Densification is faster due to capillary forces and because the transport of material is enhanced by the dissolution/precipitation mechanism. Hence, it is suitable even for hard materials which are difficult to sinter. The sintering can be called the LSP if at last two types of powder are mixed or an alloy powder is sintered. In the case of a mixture of two powders, there are several possible pathways of densification. [7]

The schematic illustration of microstructure evolution is visible in a Figure 3. In the first stage, the powder is wetted by a newly formed liquid penetrating between solid grains. There it acts as a lubricant for particle rearrangement. [7]

The mechanism of a structure evolution is different based on a dissolution property of a powder and liquid. If the powder dissolves in a liquid, solvent improves transport, increasing the speed rate of coarsening and densification. Another possibility is that a liquid is dissolved in solid, forming an alloy. Also, there is a possibility that the powder neither the liquid will be dissolved. In that case, only densification of a powder occurs, forming a solid skeleton. In case of an alloyed powder, particles are partially melted forming a semisolid structure enabling a plastic flow. [7]

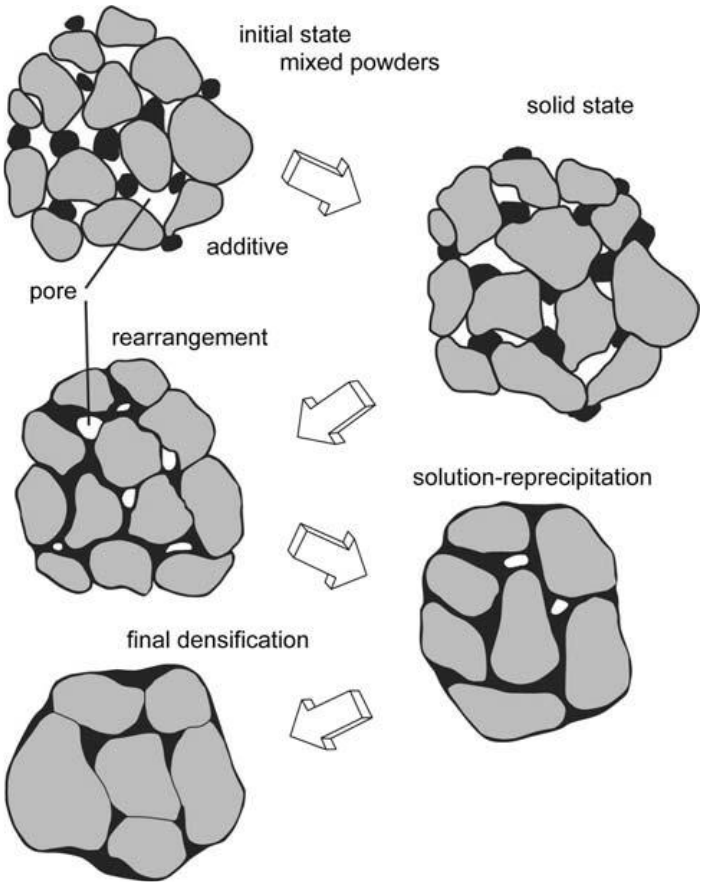

Figure 3 Schematic illustration of the LPS, from: [5]

Hot uniaxial pressing

As the name suggests this technique uses pressure to improve the sintering process. Densification is driven by a plastic flow, grain rearrangement, and stress-enhanced diffusion [8]. This method is suitable to produce high-density and performance materials. Due to a low temperature, the grain roughness is lower, so sintering is not very sensitive to the input quality of the powder. Thanks to the high-pressure method, it is also possible to prepare a covalent ceramic such as B_4C or SiC without the need for additives. But more often is this method is used in metallurgy. A disadvantage of a hot uniaxial pressing is its high price. Because sintering is processed at a high pressure and high temperatures expensive dies are required. Molds usually have a short life due to working conditions. More often they are made of ceramic rather than metal. In addition, uniaxial hot sintering is limited by the obtainable shape of ceramic, which must be simple. Therefore, uniaxial hot pressing has low productivity, so the plants do not often use it. Instead, it is frequently used in laboratories or research centers. [9]

3.2 Spark Plasma Sintering

Spark Plasma Sintering (SPS) is a technology that enables more time and energy-effective sintering. During the process, pressure is applied as in a case of high uniaxial sintering. Therefore, dies are made of a heat-resistant material. Another requirement for the die is its electric and thermal conductivity. SPS offers the same opportunity as the high-temperature uniaxial sintering but in contrast, it can achieve up to a hundred times higher heating rate. [10]

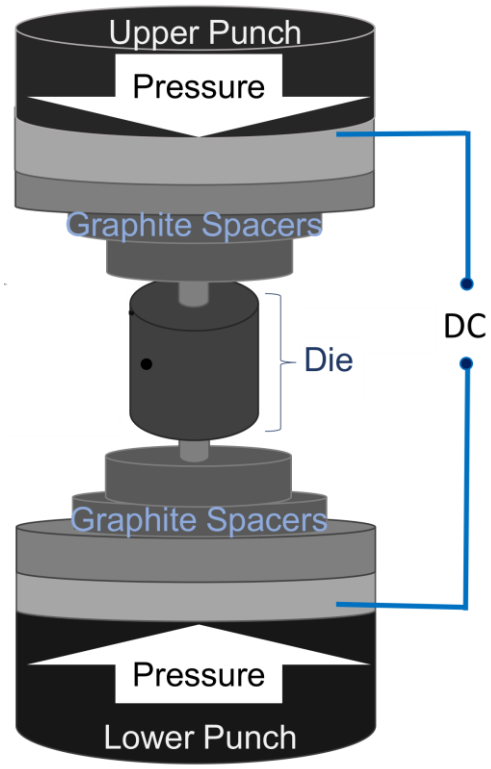

Figure 4 Schematic illustration of a conventional SPS setup, from [11]

The origin of Spark Plasma Sintering terminology is based on the putative mechanism by which heat is generated. The SPS generates DC pulses that were believed to causing a sparking discharge between particle surfaces. Such discharges can immediately raise the temperature at the contact point up to 10,000 °C. Therefore, the surface at contact zones of particles evaporates. Because the interval between pulses is long compared to the energy of one pulse, the heat has time to dissipate. Vapors condense and transfer energy to a solid, which melts and forms a necking. Many studies have focused on this topic but have not found proof for this mechanism. [10] Therefore, the most important mechanism of heat production is the Joule heat caused by the electrical resistance of a conductive die.

High-pressure SPS

The amplitude of the usable stress depends on the fracture strength of a form. Conventional SPS does not excite 100 MPa due to the graphite vessel. Graphite dies are often used due to their thermo-

mechanical properties, high electrical and thermal conductivity, low coefficient of thermal expansion, and excellent thermal shock resistance. The low service temperature of graphite in an oxidic atmosphere is not a problem, as the device is normally designed to be able to operate under inert conditions. However, the mechanical properties of graphite are still lacking due to high loads.

Therefore, a double-stage mold that combines creep-resistant, tough material and graphite is often used to solve this problem. By using silicon carbide, silicon nitride, or a tungsten carbide it is possible to achieve an impressive pressure of up to 1 GPa [12; 13]. However, these materials are expensive and difficult to machine. The work made by Salvatore Grasso et al. 2012 [14] had shown there is a possibility to reduce the cost of high-pressure dies by using a carbon fiber composite (CFC). Due to its machinability, this material is about 50 times cheaper compared to silicon or tungsten carbide. Another disadvantage of a double-stage die is the reduction of sample size. [15]

A new approach is a Belt type device designed by a team of Balima et al. 2018. This device allows the application of extreme pressure (up to 6 GPa). The belt device is not new in terms of pressure generation equipment, but its application in the SPS has been challenging. In the case of a belt punches have a conical shape, therefore have an inert face of a mold. This is to keep punches and the central part of a die-in compression. The central die and punches are also reinforced with outer rings. [13]

3.3 Hydrothermal reactions (Background)

Hydrothermal technology is generally understood as a reaction process of input materials within an aqueous solvent. The presence of elevated temperature and hydrostatic pressure is crucial. This allows the synthesis of even normally insoluble compounds. However, the definition of the technology is not consistent and often differs from author to author. Some define the temperature level to be greater than 100 °C. Different sources set the temperature to a critical point of a solution. The pressure level is generally understood to be higher than atmospheric. [16]

The synthesis is carried in a closed system, which makes it easier to control the conditions. The apparatus/autoclave must be mechanically and chemically resistant. Because highly corrosive environments often occur in the autoclave. Besides, the inner wall is separate from an aggressive solution by liners.

Despite the importance of a hydrothermal synthesis in material science and engineering, the hydrothermal phenomena have a geologic origin. It was first used to explain the formation of rock and minerals in the ocean by Roderick Murchison (1792–1871). The mechanism inspired further research that led to the development of hydrothermal methods [17]

3.3.1 Hydrothermal Sintering

In 1976 Shin-Ichi Hirano and Shigeuki Sōmiya introduced hydrothermal reaction sintering (HRS) [18]. In their work, bulk Cr_2O_3 ceramic was prepared by the reaction of a chromium powder and supercritical water.

In 1984, Yamasaki's group developed hydrothermal hot pressing (HHP). Ceramics were prepared at a pressure up to 300 MPa and temperature above 350 °C in the presence of a solvent. This method is in many ways like a CSP. It uses uniaxial pressing, but the device is sealed and temperatures are higher. This method finds its application as a method for illuminating the bio-mineralization process and as nuclear waste conserving method. [19]

Hydrothermal liquid-phase densification (rHLPS) is a pressureless technique. This method was published by Riman et al. in 2007. The technique is performed as follows: Pre-sintered samples are placed into a reaction vessel filled with a liquid agent. Usually, the temperature of sintering is above 250 °C. [19]

Hydrothermal Sintering (HS) is a low-temperature variant of Hydrothermal Hot Pressing. Like the CSP temperatures do not exceed 300 °C. The difference between HS and CSP can be seen in the picture below. HS follows the convention of an origin hydrothermal process, so it uses a hermetically sealed vessel. The tightness of a mold is often ensured by a PTFE foil. To avoid liquid being entrapped in porosity mold contains a retreat space. [20]

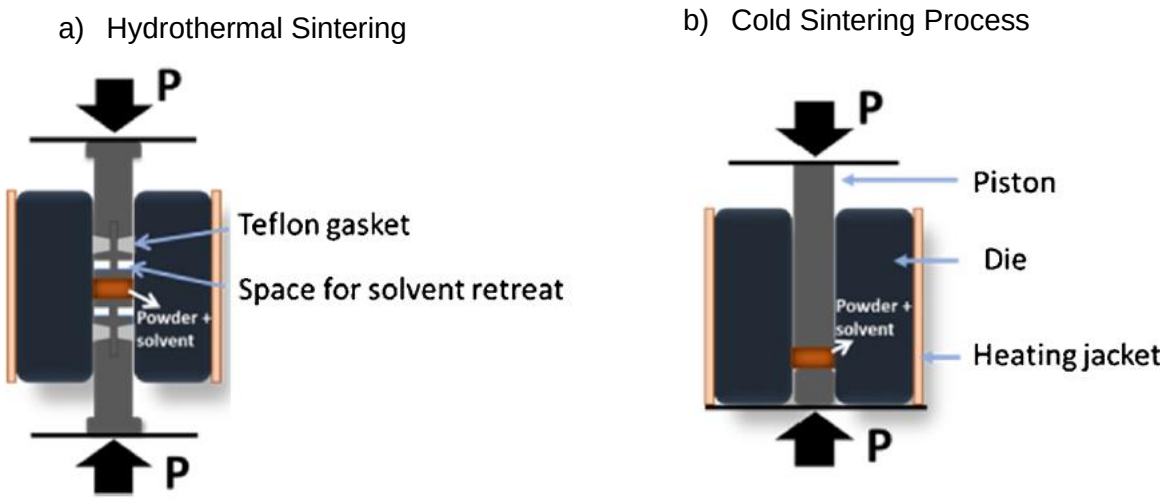

Figure 5A schematic setup of a die for a) HS, b) CSP [20]

Like an HS, it is performed in a closed system, but because the mixture is enclosed in the flexible seal there is no room for the liquid to escape. However, this method was successfully used by a group of Anna Jiang from Southwest Jiaotong University [4] for the preparation of dense silica. Dense ceramic was prepared by application of isostatic pressure as it is inclined by the title. Transparent (70 %) silica samples were prepared by a nanopowder in a solution of potassium hydroxide solution.

The Figure 6 shows a schema of cold hydrothermal-based sintering techniques.

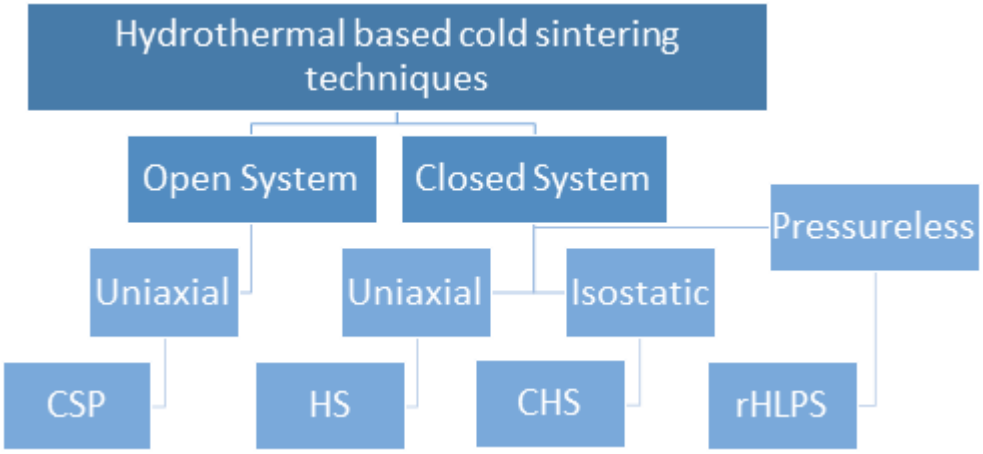

Figure 6 Comparison of low-temperature hydrothermal densification techniques, inspired by [20]

3.4 Cold Sintering Process

CSP is a novel technique. It was patented by a research group (Clive A. Randall, Jing Guo, Amanda Baker, Michael Lanagan, Hanzheng Guo) from Penn State University in 2016. CSP is a hydrothermal technique that can radically reduce the sintering temperature of ceramics. Compared to pressureless sintering this process is time-saving, the ceramic can be densified within an hour. That is the combination that leads to impressive energy and cost reduction. [21]

The CSP runs a temperature higher than 100 °C but lower than 300 °C. Because the process temperature is low, the energy for coarsening is also low. This makes the CSP ideal for preparing ceramic with a controlled grain size [22]. Conventional high sintering temperature for production of ceramic capacitors is problematic because of the degradation of a metallic conductor. Hence, devices that are prepared at temperatures around 1,200 °C requires the use of noble metals with a high melting point such as platinum or palladium. The content of a noble inevitably results in a cost increase. So, if only the cold sintering will allow non-noble metals to substitute a noble one the price of capacitors would decrease by half of a price [23].

Another advantage of a CSP is that it allows a combination of ceramic with a polymer, metal alloys with a low melting point, or any other material with low thermal stability. Such composites can find application in electrical engineering.

It should be noted that not all ceramics are suitable for this method. Ceramics have often a high chemical stability. This method is more suitable for the preparation of technical ceramics rather than high-strength ceramics. So, far CSP has been successfully used for the preparation of oxidic ceramics with some exceptions such as NaCl ceramics. [24]

Apparatus

Experimental CSP does not necessarily require expensive equipment. Dense ceramic samples can be prepared with a cheap uniaxial press in combination with a heating jacket. Challenging is to master the densification conditions. The outcome of densification depends to a large extent on several factors. In addition to the temperature and pressure program, the chemical environment must be adjusted.

Sintering mechanisms

CSP is a dissolution precipitation-based process, in which a transient liquate mediates the transport of mater. The content of the liquid phase moves around 1 – 25 wt.%. CSP is not restricted for a use of water-based solutions only. Generally, the transient liquid can be anything if it reacts with a powder in a convenient way. It is possible to use organic alcohols, ketones, esters, molten salts, or hydroxides. [25]

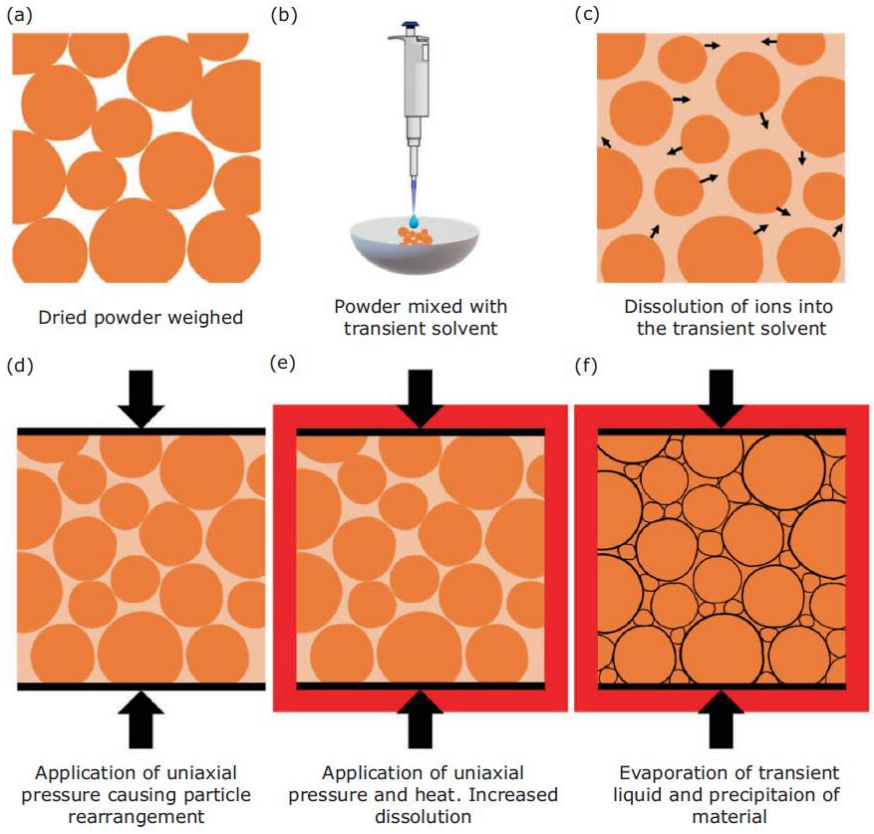

Figure 7 Illustration of dissolution/precipitation mechanism during the CSP, from: [26]

The residual content of the solvent is generally undesirable. Hence, it is advantageous to choose such an agent with can be easily removed. The boiling point or the decomposition temperature of the solvent should be close to a processing temperature (100-300 °C) so, the liquid can evaporate. Otherwise, a small amount of phase will always be present in a porosity. [27]

Easy escape of a liquid phase is desirable for a couple of reasons. First, the sealed liquid can obstacle the compaction. Second, the liquid phase can modify the properties of the ceramic.

Dissolution and precipitation are a process which is related to a surface only. That means, only particle coarsening should occur. This problem was explained by the role of stress gradient. Which is generated by a uniaxial pressing and a limited contact of particles. In the literature was claimed: *"*Consider the simplest model, in which two 10-μm spheres of material with an elastic modulus of 200 GPa have compressed axially at a reasonable pressing pressure of 200 MPa. At the contact point, the Hertzian contact stress is more than 20 GPa." [28]

This description is in a simplified way but it is a helpful promotion to a better understanding of a problem. The surface tension may vary across a single grain in an order of magnitude. The applied pressure at a contact point of two-particle results in an increase of solubility. So-called pressure solution then leads to mass transport to an area with a lower level of stress. The pressure solution is affected by several factors, such as the difference between compressibility and polarity, so there may exist some

exceptional combination of solid and solvent. But this should not be a case of an aqueous solution. It is generally expected that temperature will increase solubility. On the other hand, there are some exceptions when the solubility decreases. [19]

The process

In the first stage, added liquid forms a layer of lubrication as well as a dissolution agent. Because dissolution is faster on sharp edges of particles, they become more spherical. Making them easier to coordinate them into a more space-efficient structure. The effects of lubrication increase the initial relative density but do not cause necking. [16]

Depending on the chemistry of both solvent and a powder two types of dissolution can occur. More favorable is congruent dissolution which means that the ratio in which components are addressed is stochiometric.

In the case of an incongruent dissolution, the components have a different dissolving kinetic. One of the components is dissolved faster making the surface passive to the next reaction. This problem can be solved by using a more aggressive reactant or a reagent that has previously been saturated with the easily solvable component (See the Figure 8). This method reduces, the dissolution kinetics of a more reactive component. Although the solubility of a second phase does not decrease dramatically. A similar tactic is possible for a material that has negligible solubility. If the solvent contains a component suitable for precipitation of a solid phase. [25; 29]

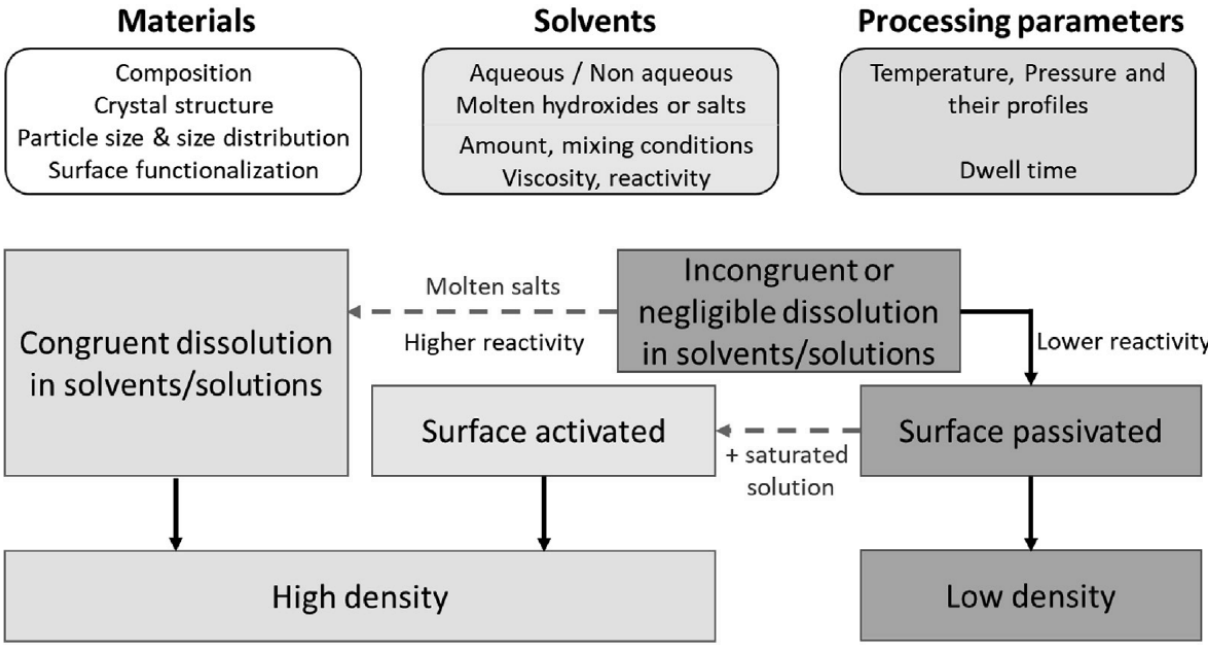

Figure 8 Schematic diagram of a CSP mechanism, from: [25]

Phase precipitation follows the formation of an oversaturated solution, which could be initiated by several factors, such as: evaporation of liquid, a strain gradient, and a temperature gradient. In some

cases, gelation may occur. This appears more frequently if the solution is saturated quickly. Gelation causes a disorder in a grain boundary. [28]

Another mechanism may take place during cold sintering. Marangoni flow takes place at a liquid-liquid interface. This mechanism expects a different concentration of a compound near the area of the contact points. That leads to the existence of surface tension on the surface of liquids [29]. In some cases, solid reacts with a liquid to form layer solvable salts or hydroxides. This new phase has generally lower mechanical properties. If the yield strength is low enough a plastic flow may occur and the densification process will be increased significantly. [19]

Zinc oxide

Zinc oxide is commonly known as a white powder, which is often used as a pigment. This material is widely used in the field of additives: concrete, automotive tires... It is used in the pharmacy and food sector. Zinc oxide has a piezoelectric property due to its wurtzite structure [16]. It is an n-type semiconductor with a bandgap of 3.3 eV. For that reason, zinc oxide is suitable for many electrotechnical devices, such as varistors, gas sensors, field-effect transistors (FET), and Surface Acoustic Wave (SAW) devices. Another result of zinc oxide bandgap is its optical properties. Zinc monocrystal is transparent to visible light. It is luminescent material – it emits light when it is disposed to a wavelength around 370 nm.

Demonstration of a sold sintered ZnO was first published by Shuichi Funanhashi et al. in 2016. They successfully prepared a dense ceramic at a low temperature (88–300 °C) in presence of an acetic acid solution [30]. The authors reported an increase in grain size see – the **Chyba! Nenalezen zdroj odkazů.**. The sintering in a presence of acetic acid is temperature dependent with a breaking point at 50–90 °C [31].

Different research Benjamin Dargatz et al. 2016 have reported successful low sintering of the ceramic even in pure water. Although due to the sintering temperature of 400 °C this sintering cannot be considered as a CSP [32]. Xiaoyu Kang et. al. observed that the ZnO cannot be sintered in HCl, H_2SO_4, $ZnCl_2$, and $ZnSO_4$ although the ZnO has a good solubility. Due to a formation of secondary phases that consumes the transient liquid [31].

The mechanical properties of a cold sintered zinc oxide were studied by Sarah Lowum et. al. The research group used a Ball on three ball method for receiving a Weibull distribution. Authors reported Weibull distribution of characteristic strength of [61.8–67.1] MPa and Weibull module of [6.1–10.0]. Which seemed to be a lower standard for a conventionally sintered ceramic. However, the comparison is problematic since authors find difficult to find a representative reference. [33]

Barium titanate

Barium titanate is a substitution for a lead-based perovskite due to the harmful effect of lead on living organisms. $BaTiO_3$ was the first recognized ferroelectric perovskite. It has three Curie temperatures and three related ferroelectric phases: rhombohedral which exists below a -90 °C, orthorhombic (from -90 to 5 °C), tetragonal (5–120 °C). Besides, barium titanate has other nonpolar forms at elevated temperatures: Cubic (120–1,460 °C) and hexagonal. [23]

The $BaTiO_3$ is suitable for the manufacture of ceramic capacitors because of it has exceptionally high dielectric constant. Dielectric properties increase with a temperature up to a Curie temperature (1,200 → 12,000 at 1 kHz). Because of this variation in properties, the ceramic is not used in a pure form. The high resistivity appears at a narrow interval of temperature near a Curie point but these temperatures are too high for an ordinary application. Fortunately, the electric properties of barium titanate can be effectively tailored by doping. $BaTiO_3$ easily forms a solid solution with other titanates such as $PbTiO_3$ or $SrTiO_3$ and other oxides (ZrO_2 or SnO_2). With the right additive, the ceramic may perform semiconductive properties. [23]

Because of the large versatility of barium titanate, it can be used as capacitors or piezoelectric piezoceramic devices such as electrochemical transducers, high-voltage generators, electromechanical, resistors … [23]

Barium titanate is an example of an incongruently solvable material, hence the densification by a CSP is problematic. One of the approaches was presented by the team of Hanzheng Guo (2016) who successfully prepared the ceramic from nanopowder with a low addition of rutile TiO_2. As a solvent, an aqueous solution of anhydrous $Ba(OH)_2$ was used at a concentration of 0.1 M [29]. This technique is much the same as a hydrothermal synthesis of $BaTiO_3$ from a TiO_2 powder when the barium titanate. When the powder is a result of a reaction between rutile and a hydroxide. The reaction is illustrated in the Figure 9. [17]

The ceramic was prepared at a very high pressure of 430 MPa but a notably low temperature of 180 °C. The maximal received density was up to 95 %TD. Because of barium carbonate formation, during a sintering, additional annealing at a temperature around 900 °C was important. [29]

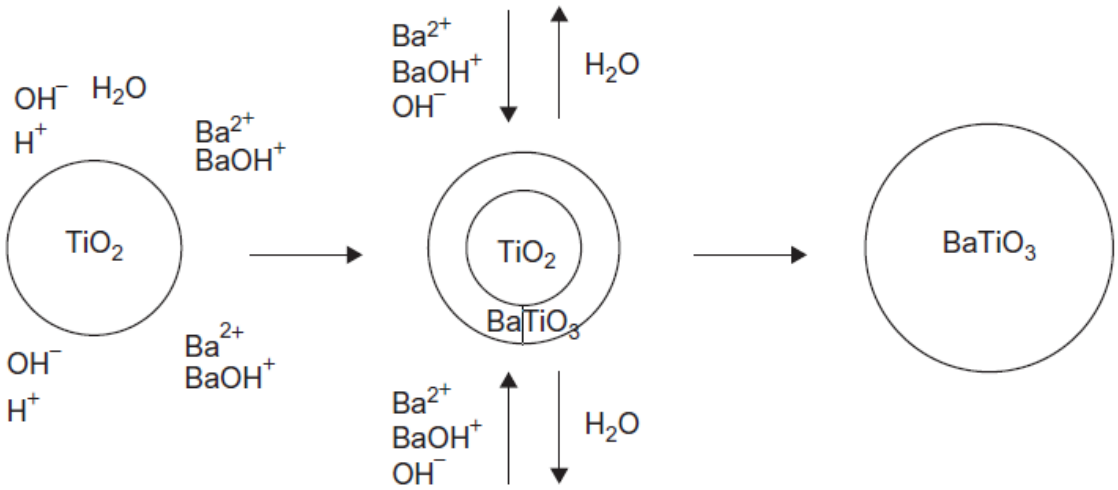

Figure 9 Illustration of a dissolution precipitation reaction between TiO_2 powder and BaOH, from [17]

A different approach was used for the densification of a $BaTiO_3$ / PTFE composite by Takao Sada et. al. (2020). In this case, additional TiO_2 powder was substituted by an amorphous TiO_2 layer on $BaTiO_3$ particles which was formed by soaking the powder in hot acetic acid. The soaking leads to an incongruent dissolution of barium titanate which is visualized in the Figure 10. Barium oxide octahydrate was used as a solvent. Besides, the authors added PTFE (from 2.5 up to 20 wt.%), to enhance electric properties. Since the PTFE particles were present, the ceramic was not further annealed (at 900 °C), instead, samples were sintered at 225 °C for an hour and baked at 200 °C. Authors reported a significant improvement in the functional properties of the composite. They found a decrease in loss tangent and increase in permittivity. [34]

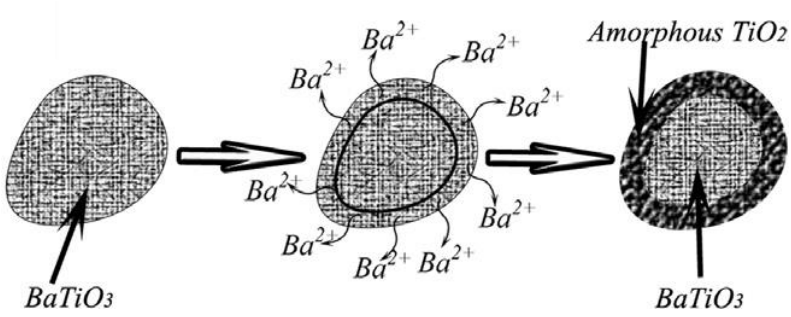

Figure 10 Illustration of incongruent dissolution of $BaTiO_3$ and a formation of amorphous TiO_2, from [28]

The possibility of doping through the CSP was studied by Sada Takao et. al. (2020): The principle of sintering was quite similar to previous research, however the $Sr(OH)_2$ was used as a transient solvent/flux instead of a barium hydroxide. The doping mediator was expected to lower the Curie temperature. The research team prepared a dense ceramic with a theoretic density of above 90 %TD. They also prepared an EDS mapping of FIB-prepared samples. Mapping has shown Ti and Ba atoms were distributed homogenously in the ceramic but Sr atoms occupied grain boundaries only. Besides the

Sr content also alter with a boundary orientation in a manner that the boundaries which were more perpendicular on an applied pressure have a lack of strontium (See the Figure 11). That leads to a heterogeneous crystal structure and distribution of $Ba_{1-x}Sr_xTiO_3$. [35]

Kosuke Tsuji et. al. solved the problem with an incongruent dissolution of Ba ions by using an aggressive 1:1 NaOH and KOH solvent molar solution was used. The authors received a theoretical density of up to 99 %. [27]

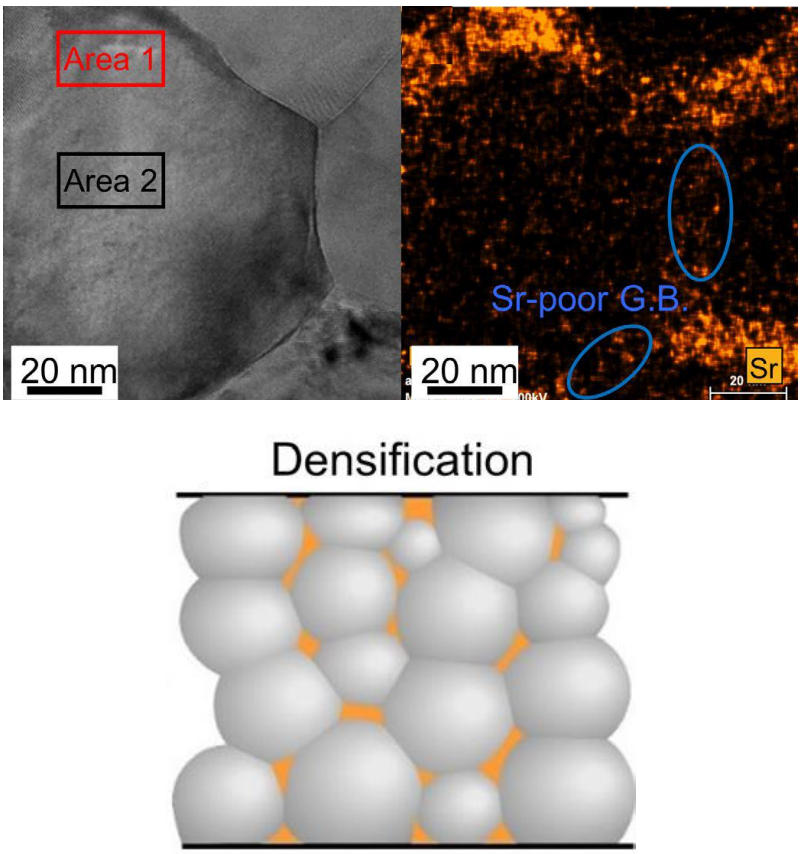

Figure 11 Strontium distribution after cold sintering [35]

4 EXPERIMENTAL PART

4.1 Spark Plasma Sintering Device

The zinc oxide and barium titanate ceramic samples were prepared using SPS - 625 Furnace (Fuji Electronic Industrial Co., Ltd., Japan). This device was chosen for its complex data outcome and adjustability. During sintering, the device measured a temperature, load, and dilatation by a frequency of 1 s. A vacuum chamber with a barometer was used for the detection and measurement of gas generation. The temperature data were Expected advantages of the SPS high-pressure die are higher available temperature and pressure (500 MPa) plus unique ability to detect exits of gasses in a vacuum.

Figure 12 SPS-625 furnace

4.2 Design of the high pressure die

Graphite dies are frequently used for Spark Plasma Sintering because they have an excellent thermomechanical property. Its short-term tensile and compressive strength increase with a temperature up to 2,000 °C, but above 2,400 °C the mechanical stability is compromised by the creep. Graphite has a high thermal shock resistance because it has high thermal conductivity and a low coefficient of linear thermal expansion. Besides, graphite has a high electric conductivity which is important for the SPS. [37]

One drawback of graphite is its low oxidation resistance, so it burns at a temperature above 400 °C if the oxygen is present. Hence, SPS is performed in a vacuum or inert atmosphere. The thermal stability of the carbon is not limited. Another problem is the relatively low strength and hardness of the material. For that reason, two types of dies were used during a sintering process.

Limitations of the materials and constructions

Mechanical stability is one of the main aspects and carbon, silicon carbide, tungsten carbide (WC-Co), silicon nitride (gas pressure sintered) were considered. The selection was compared with the literature [12].

Chemical stability is important due to the high corrosion activity of water and acids involved in the cold sintering process. During the heating, these corrosive compounds are usually exiting the sintering die around the punches. Carbon is highly corrosion resistant to water or acids.

Electrical and thermal conductivity are also important parameters and two main factors must be considered:

- The electrical conductivity of the sintering die can cause welding of the punches and the cylinder; therefore, it is suitable to isolate the sintering die or use non-conductive materials. However, the electrical conductivity of the outer die is very high compare with metals.
- Thermal conductivity is important because heat is generated in the graphite die and the temperature is measured on the outer surface by the thermocouples inserted in the small cavity.

Sintered wolfram carbide is a material typically used for wear-resistant parts (cutting devices, nozzles, draw dies, drills…). Hardmetal has a good mechanical property, toughness, shock resistance, and relatively good thermal conductivity Typical tungsten carbide with a binder is sintered by LPS where the second phase is cobalt, molybdenum, or a nickel. A disadvantage of cobalt-based tungsten carbide is its relatively low corrosive resistance of cobalt in the corrosive environment. Nickel-based wolfram carbide has a better corrosion electrochemical corrosion resistance, due to the tendency to self-passivation. [36]

Silicon carbide is a hard and rigid material with excellent thermal conductivity and low thermal expansion. It also has very good chemical resistance. Therefore, this material is commonly used for bearings, nozzles, high temperature applications…

Low-pressure vessel

Graphite form (visible in the Figure 13) was used for low-pressure sintering (up to 50 MPa). The cylinder had a diameter of 35 mm and 30 mm high. The hole for a piston had a 12 mm in diameter.

High-Pressure vessel

To reach a higher-pressure combination of a graphite and SiC die was used. Because of their compression strength, mismatch dies were separated by an interface disc made of silicon nitride. A cylindrical space was machined on a surface of silicon punches, so the silicon nitride discs were well embedded. The diameter of punches decreased by the way to the center of the die. The effective conversion of the pressure was in a ratio of 1:6.6 when the 26 mm spacing disc is used. Meaning the maximal achievable pressure is related to a compressive strength of graphite punches.

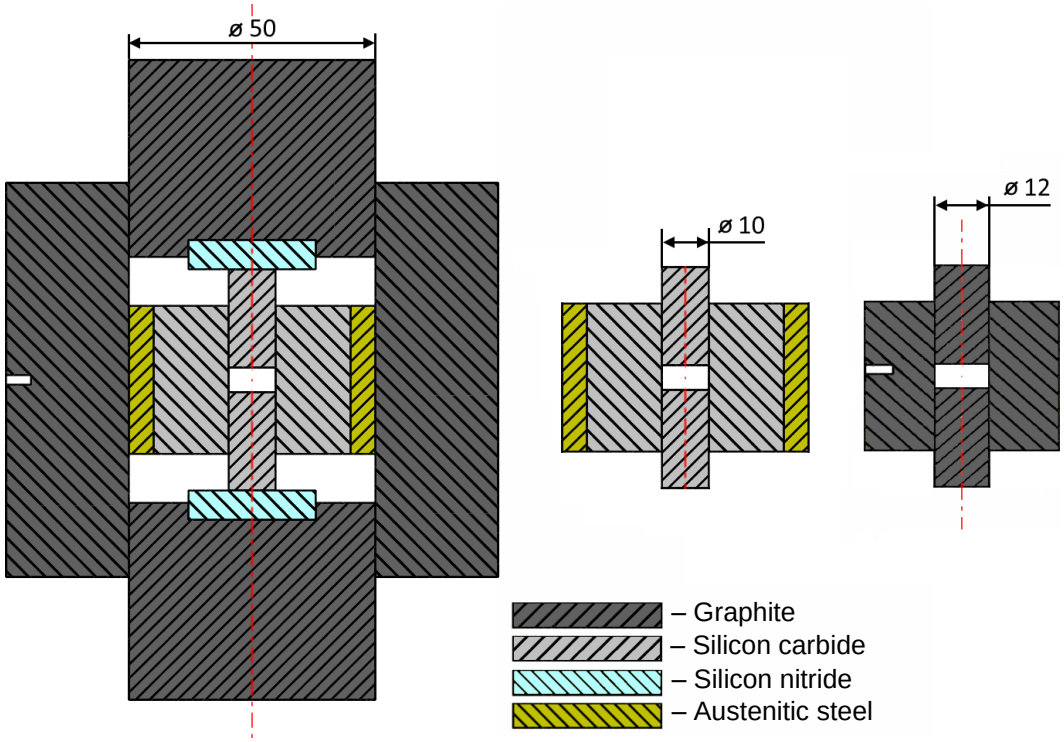

Figure 13 Design of an SPS dies, the composite die is at the left side of a page the standard low-pressure one is on the right

Since the CSP uses a wet powder there was a serious risk of rupture of a vessel. Therefore, the ceramic was reinforced by an austenitic steel (material number:1.4301) ring.

Table 1 Compressive strength of materials and expected pressure, reference: a) [38], b) [40], c) [39], d) [41]; e) on contact with C/SiC punch

Part	Expected pressure [MPa]	Compressive strength [MPa]	Thermal conductivity [$W \cdot m^{-1} \cdot K^{-1}$]
Graphite (Outer punch)	74[e)]	167[a)]	81 [a)]
Silicon nitride (Spacer)	500[e)]	3,000[b)]	21 [b)]
SiC (Punch)	500	3,500[c)]	115 –190 [c)]
WC (Punch)	500	3,347[d)]	28 – 88 [d)]

Assembly of the outer ring on the cylinder

The temperature of an assembly was predicted according to a calculation located in an Appendix (Calculations for the cylinder assembly). The ceramic part of a form was placed inside the muffle. The program was set to a temperature of 550 °C with a heating rate of 20 $°C \cdot min^{-1}$. To avoid damage to the ceramic caused by a thermal shock ceramic stayed present in the muffle for the entire heating cycle. The steel ring was placed in a preheated muffle when the temperature reached its maxima to avoid oxidation. After 20 min dwell the ring was pulled on the ceramic.

Preparation of segments cylinder

The SSiC (Sintered Silicon Carbide) die and a set of punches were bought from CeramTec (CeramTec Czech Republic, s.r.o.). The die had 40 mm in diameter and was 30 mm high.

A 30 mm long piece of a seamless pipe (Nerezové Materiály, s.r.o.) with an outside diameter of 50 mm and wall thickness of 5 mm was cut by an angle grinder. Then the internal face was turned to match an estimated parameter. Graphite forms were ordered from a Mersen (Mersen, France).

4.3 Cold Sintering

ZnO nanopowder

Sets of specimens were prepared by the sintering of a zinc oxide nanopowder (50 nm, 99.7 %, Inframat® Advanced Materials LLC, USA). The sintering conditions varied by heating rate, dwell temperature/time, maximal pressure, and liquid content. Two possible ways of sealings were tested: graphite paper (Graphite) or aluminium foil (Aluminium).

Table 2 The list of sintered samples, Name of each sample is based on: powder, solution (Acetic acid/Aqua/Hydrochloric acid), total temperature/heating rate, and applied pressure, the SPS No. (Spark Plasma Sintering number) is the catalog number referring to a sintering record. The concentration of a solution is not mentioned in the list, but a 1 M solution was always used in the case of acetic acid. The concentration of hydrochloric acid was 35 %wt.

Preliminary sintering of $BaTiO_3$

Preliminary sintering of barium titanate nanopowder (cubic, 50 nm, 99.9 %, Sigma Aldrich® Merck KGaA, Darmstadt, Germany) prepared to pre-test sintering possibilities. An aqueous solution of acetic and hydrochloric acid was used as a solvent. Table 2 describes the sintering parameters of an experiment.

Powder preparation

Three techniques were used to wet the powder before loading it into the sintering die:

1. Stirring in the mortar – wetted powders were prepared by mixing a liquid with a powder inside a mortar and pestle. The weight fraction was measured by a laboratory scale.
2. Drop wetting – dry powder was pre-pressed by 80 MPa and drops of the acid solution were dropped on the pellet. The final content of the acid solution in the pellet was verified by weight.
3. Diffuse wetting – preformed samples were placed between two slides of filter paper. These papers were previously moistened with a solvent. The wetting took several hours depending on how much liquid content was required and by weight the final content of the solvent was determined.

Special sealing (Aluminium)

Some samples were enclosed in a capsule from an aluminium foil for the study of a liquid escape. Standard household foil 0.016 mm thick was shaped in a form of crucibles (Figure 14) and filled with a pre-pressed powder.

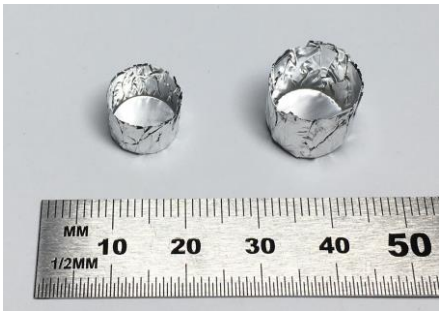

Figure 14 Aluminium foil crucibles, variants for both dies

Sintering

1.5 or 1 g of wetted powder was placed inside the die (ø 10 and 12 mm) and preloaded by a hand-operated press. Then the vessel was completely assembled and placed inside the SPS furnace. The temperature was controlled by a thermocouple, which was mounted in the cavity on the outside surface of the graphite die. During the first two minutes, the load reached its maximum by then the SPS chamber was turned on. The temperature was held at ambient temperature for 10 minutes, the first 2 minutes mechanical pressure was applied and the following 8 minutes chamber was evacuated up to approximately 10 Pa. The vacuum (running vacuum pump) prevented the sintering die against oxidation and allowed the measurement of vapor escape. The SPS device has recorded during each sintering cycle an applied load, electric current and voltage, vacuum data, and displacement. These data are accessible for each SPS run.

Table 2 The list of sintered samples, Name of each sample is based on: powder, solution (Acetic acid/Aqua/Hydrochloric acid), total temperature/heating rate, and applied pressure, the SPS No. (Spark Plasma Sintering number) is the catalog number referring to a sintering record

Name	Powder	Maximal temperature [°C]	Heating rate [°C·min^{-1}]	Dwell time [min]	Maximal pressure [MPa]	Solvent	Solvent fraction [%]	Soaking time [min]	Wetting technique	Die design	Sealing	SPS No.
Znxx_30/1_05_1081	ZnO	300	10	60	50	None	-	-	-	Low pressure	Graphite	1081
ZnAq_30/1_05_1203	ZnO	300	10	60	50	Aqua de.	20	"30"	Standard	Low pressure	Graphite	1203
ZnAq_30/1_05_1220	ZnO	300	10	60	50	Aqua de.	10	"20"	Standard	Low pressure	Graphite	1220
ZnAq_30/1_30_1236	ZnO	300	10	60	300	Aqua de.	15	"60"	Standard	High pressure	Aluminium	1236
ZnAq_30/1_30_1257	ZnO	300	10	60	300	Aqua de.	20	"30"	Standard	High pressure	Aluminium	1257
ZnAq_30/3_05_1224	ZnO	300	27	60	50	Aqua de.	10	"10"	Standard	Low pressure	Graphite	1224
ZnAq_30/3_05_1225	ZnO	300	27	60	50	Aqua de.	15	"10"	Standard	Low pressure	Graphite	1225
ZnAc_30/1_05_1102	ZnO	300	5	38	50	AcOH	20	30	Standard	Low pressure	Graphite	1102
ZnAc_30/1_05_1070	ZnO	300	10	60	50	AcOH	20	30	Standard	Low pressure	Graphite	1070
ZnAc_30/1_05_1079	ZnO	300	10	60	50	AcOH	20	5	Standard	Low pressure	Graphite	1079
ZnAc_30/1_05_1080	ZnO	300	10	60	50	AcOH	20	30	Standard	Low pressure	Graphite	1080
ZnAc_30/1_30_1160	ZnO	300	10	60	300	AcOH	20	60	Standard	High pressure	-	1160
ZnAc_30/1_30_1165	ZnO	300	10	60	300	AcOH	20	45	Standard	High pressure	-	1165
ZnAc_30/2_05_1204	ZnO	300	20	60	50	AcOH	20	30	Standard	Low pressure	Graphite	1204
ZnAc_30/3_05_1226	ZnO	300	27	60	50	AcOH	24	240	Diffusion	Low pressure	Graphite	1226
ZnAc_30/3_05_1228	ZnO	300	27	60	50	AcOH	10	120	Diffusion	Low pressure	Graphite	1228
ZnAc_30/3_05_1290	ZnO	300	27	60	50	AcOH	20	40	Standard	Low pressure	Aluminium	1290
ZnAc_30/3_05_1291	ZnO	300	27	60	50	AcOH	20	45	Standard	High pressure	Aluminium	1291
ZnAc_30/3_30_1273	ZnO	300	27	30	300	AcOH	20	45	Standard	High pressure	Aluminium	1273
ZnAc_30/3_35_1307	ZnO	300	27	60	350	AcOH	5	50	Standard	High pressure	Aluminium	1307
ZnAc_18/3_05_1199	ZnO	180	30	60	50	AcOH	20	30	Standard	Low pressure	Graphite	1199
ZnAc_24/3_05_1198	ZnO	240	30	60	50	AcOH	20	30	Standard	Low pressure	Graphite	1198
ZnAc_30/3_05_1101	ZnO	300	30	60	50	AcOH	20	30	Standard	Low pressure	Graphite	1101
ZnAc_30/3_30_1166	ZnO	300	30	60	300	AcOH	20	30	Standard	High pressure	-	1166
ZnAc_30/5_05_1100	ZnO	300	54	60	50	AcOH	20	30	Standard	Low pressure	Graphite	1100
ZnAc_30/5_05_1205	ZnO	300	54	60	50	AcOH	20	30	Dropping	Low pressure	Graphite	1205
ZnAc_30/5_05_1206	ZnO	300	54	60	50	AcOH	20	30	Dropping	Low pressure	Graphite	1206
ZnAc_30/5_05_1207	ZnO	300	54	60	50	AcOH	20	110	Dropping	Low pressure	Graphite	1207
ZnAc_30/5_05_1235	ZnO	300	54	60	50	AcOH	20	30	Standard	Low pressure	Aluminium	1235
BaAq_30/1_05_1244	BaTiO3	300	10	60	300	Aqua de.	10	"30"	Standard	High pressure	Aluminium	1244
BaAc_30/3_05_1275	BaTiO3	300	27	30	300	AcOH	10	45	Standard	High pressure	Aluminium	1275
BaCl_30/3_05_1294	BaTiO3	300	27	30	50	HCl	20	10	Standard	Low pressure	Graphite	1294

The description of sintering conditions is listed in the Table 2 The list of sintered samples, Name of each sample is based on: powder, solution (Acetic acid/Aqua/Hydrochloric acid), total temperature/heating rate, and applied pressure, the SPS No. (Spark Plasma Sintering number) is the catalog number referring to a sintering record. For a better understanding of a name convention, a sample with the code ZnAc_30/1_05_1070 will be divided into four parts (I.-IV.).

I.	II.	III.	IV.
ZnAc	30/1	05	1070

I. The Zn at the beginning of a code means that ZnO powder was sintered (Zn – ZnO, Ba – $BaTiO_3$). The solvent (Ac – Acetic acid, Aq – demineralized Aqua, Cl – hydrochloric acid, xx – no solvent) is described by the following two letters.

II. The second segment contains the temperature cycle during sintering which is described by an isothermal temperature and heating rate. The data format is the following: TT/r, where TT is the temperature in tens of °C. Analogically r is a heating rate in tens of °C per min. The heating rate was rounded to avoid decimal points (27; 54 $°C \cdot min^{-1}$). This means that the following sample was heated by 10 °C per minute up to a temperature of 300 °C and kept on the temperature for an hour.

III. Since the applied load was constant during the process the pressure could be described by maximal pressure. Pressure is encoded in tens of MPa similar to tens of °C in case of a total temperature. that means the sample was prepared by a 50 MPa.

IV. Last digits were selected to distinct samples with a similar sintering condition. They do not hold any information in the case of the thesis, but they are an important clue for orientation in sintering records.

Observing of gas exit from the sintering die

Data describing vacuum changes and dilatation were affected by the evacuating of the chamber. Therefore, a reference sintering program was prepared for each sintering condition in an absence of liquid or a sample. These data, describing the background, were subtracted from measurements. The pressure inside the SPS chamber was recorded in voltages and observed directly on the SPS apparatus in Pa, so the conversion of the recorded data was needed. Nine pairs of values were measured in an interval from 3.5 to 83,000 Pa according to a digital barometer on the SPS apparatus. Measured data are shown in a Figure 15, values are placed in the logarithmic scale. The approximation was the linear function and the equation was used for the conversion of recorded data.

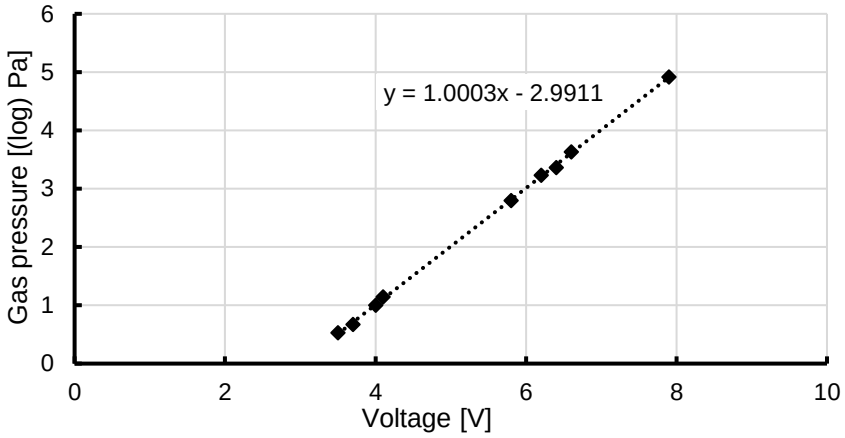

Figure 15 Gas pressure vs voltage dependence

Displacement – density conversion

The background was subtracted from the original displacement data, and with an assumption of the constant diameter of the sample, the densification was calculated. To do so final weight m_f, height h_f, and relative density ϱ_f of the sample were measured. The density development was calculated by an Equation 2.

$$\rho = \frac{m_f}{A_i \cdot (h_i - h)} \qquad (2)$$

Where m_f is mass, A_i initial area, and h_i initial height, and h final height.

The initial height of a sample was induced from the value of displacement and density when the sintering process was finished.

$$h_i = \frac{\rho_f \cdot m_f}{A_i} - h_f \qquad (3)$$

4.4 Analysis

Density measurement

Dense samples were measured by using the Archimedes method. Samples that were not suitable for this method, because of low density and open porosity, were evaluated by a geometrical method. The density of a sample was measured using Mettler XS 105 which has an accuracy of 10^{-4} g. The samples were not placed under the infrared lamp because of a risk of a subsequent change in microstructure due to a low temperature of processing. This would affect the results of following study of a microstructure by a SEM. Hence the density was measured for wet samples. The device calculated the density by comparing the mass of a sample in air m_A and the auxiliary liquid (water) m_L by using the Equation 4. The density of a liquid ϱ_L and air ϱ_A were recalculated concerning a current room temperature.

$$\rho = \frac{m_A}{m_A - m_L} \cdot (\rho_L \cdot \rho_A) + \rho_A \qquad (4)$$

SEM

Selected samples were scoped by SEM FEI Verios 460 L. To avoid coarsening due to thermal etching samples the microstructure was scoped on a fractured surface without conductive coatings if it is not stated otherwise.

SPS data recorder

The electrical current, voltage, temperature, gas pressure (in V), shrinkage, applied force, and time was recorded during each SPS run. The obtained data were used for the calculation of density development and vacuum changes.

5 RESULTS

In the following texts, results are related to a cold sintered zinc oxide (except the chapter…) ceramic which was processed in an SPS dies which were characterized in chapter 3.2 – Design of the high pressure die.

5.1 Effect of a transient liquid

Samples, that were sintered with a presence of water, had a higher relative density than the one sintered from a dry powder. However, even better results were obtained when a 1 M acetic acid was used instead of DM water, see Table 3.

Table 3 Comparison of sample densities, samples prepared by the same sintering temperature of 300 °C, pressure 50 MPa but with a different amount and type of transient liquid

Name	Heating rate [°C·min^{-1}]	Solvent	Solvent fraction [%]	Soaking time [min]	Relative density [%]
Znxx_30/1_05_1081	10	None	-	-	51
ZnAq_30/1_05_1203	10	Aqua de.	20	"30"	79
ZnAq_30/1_05_1220	10	Aqua de.	10	"20"	79
ZnAq_30/3_05_1224	27	Aqua de.	10	"10"	84
ZnAq_30/3_05_1225	27	Aqua de.	15	"10"	77
ZnAc_30/1_05_1102	5	AcOH	20	30	99
ZnAc_30/1_05_1070	10	AcOH	20	30	98
ZnAc_30/1_05_1079	10	AcOH	20	5	95
ZnAc_30/1_05_1080	10	AcOH	20	30	99
ZnAc_30/2_05_1204	20	AcOH	20	30	96
ZnAc_30/3_05_1101	30	AcOH	20	30	99
ZnAc_30/5_05_1100	54	AcOH	20	30	98

The increase in a relative density was accompanied by a grain growth as visible in the Figure 16. The temperature of 300 °C is too low for the densification of pure zinc oxide. The grain size of the powder is equivalent to a grain size of an original powder (~50 nm).

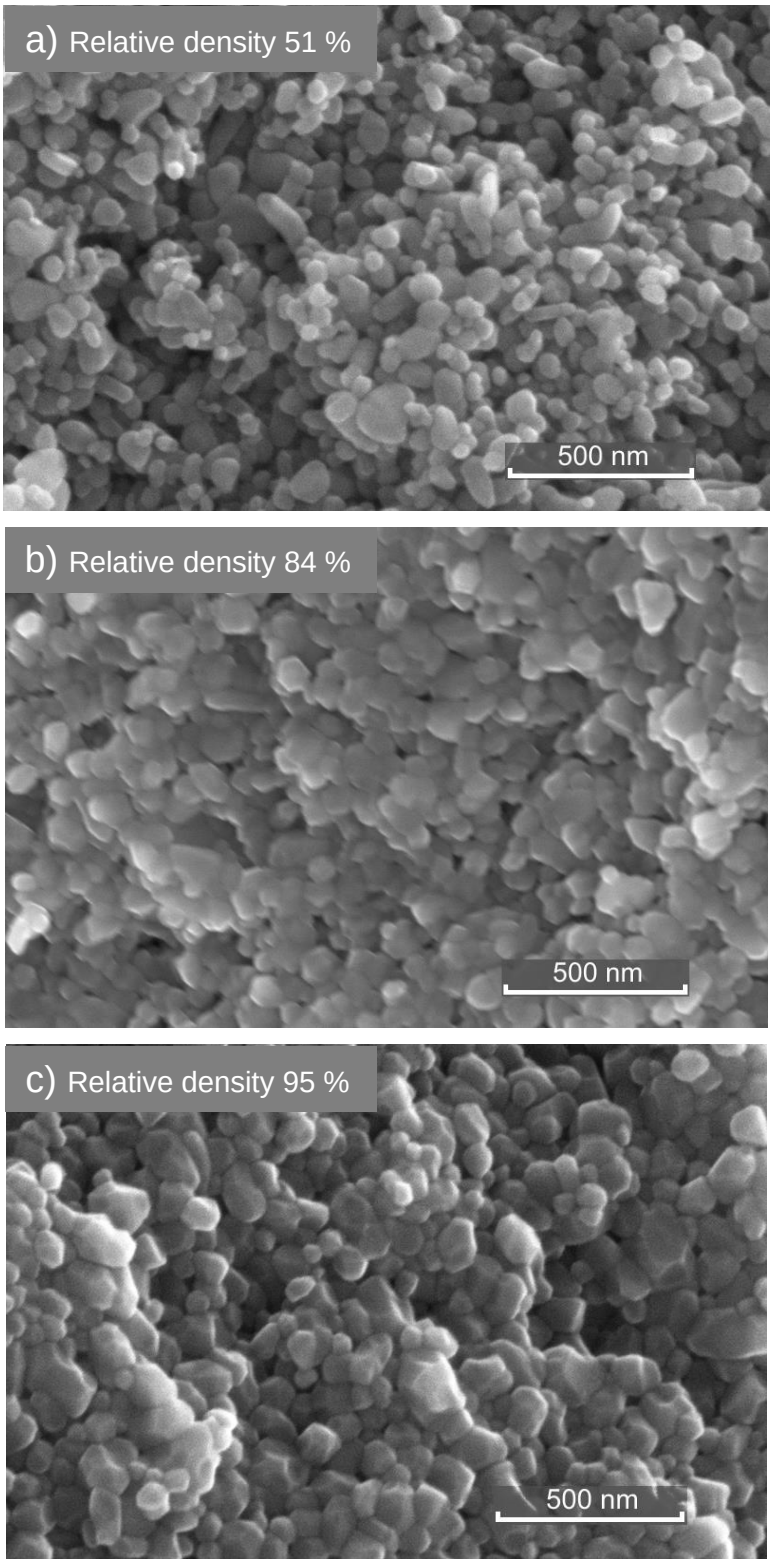

Figure 16 Microstructure of samples prepared by 50 MPa, 300 °C, a) sample without a solvent, b) sample with the addition of a 10 wt.% of water, c) sample prepared by a 20 wt.% of 1 M acetic acid

5.2 Methods of solution implementation

A diffusive wetting of a powder showed to be insufficient and lead to inhomogeneous densification. So, the rim of the sample was sintered differently than the core. Such an inhomogeneous sample was studied by a scanning electron microscope. The sample ZnAc_30/3_05_1228 (Figure 17) was broken apart in the middle and the fracture surface was sputtered by carbon to secure a conductivity of a sample. Then the sample was scoped by an electron microscope.

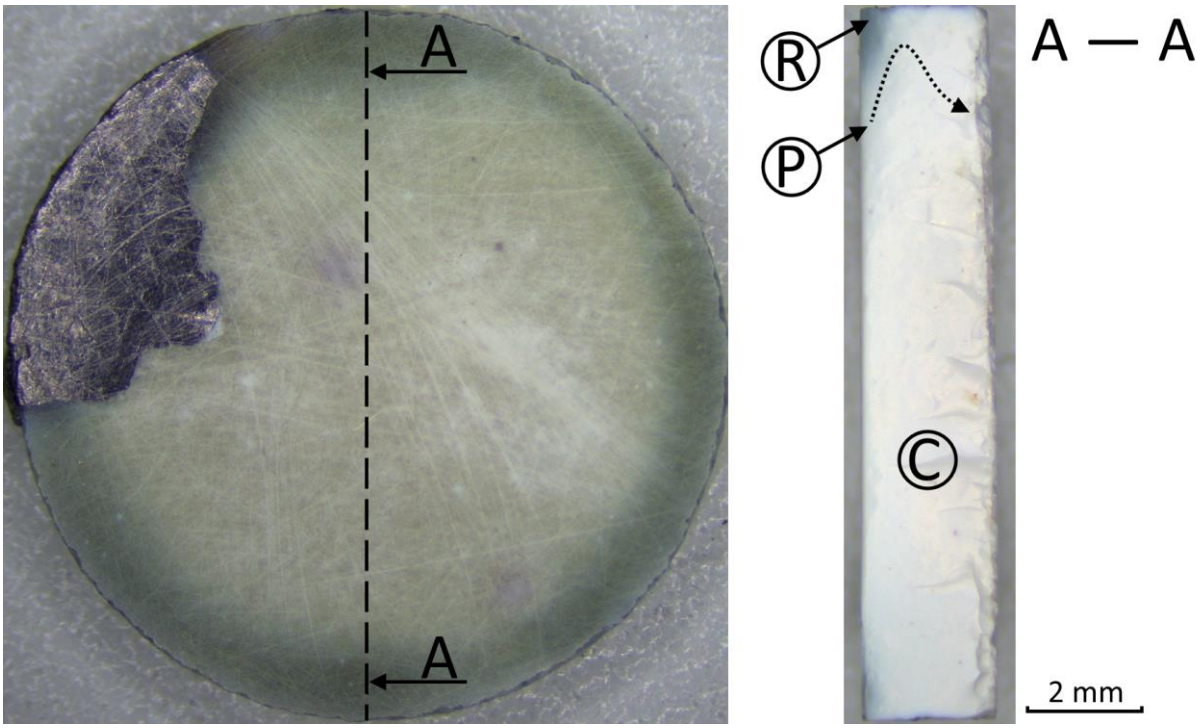

Figure 17 The studied cross-section of a sample ZnAc_30/3_05_1228, Areas R, P, C were magnified to study the structure in the dense part, center, and on the pathway between

According to SEM observation of microstructure, all parts have residual porosity. The total density of this sample was 83 % of TD (ZnAc_30/3_05_1228) and the sample with a longer soaking time reached 90 % of TD. The rim part of the sample location R was more densified as it was indicated by darker color (Figure 17). On the contrary, the core part with light green-blue color has lower density as was verified by SEM analysis, see Figure 18. The smoothly gradient structure was observed during examination of the path P (Figure 18), no crack or microstructure inhomogeneities were observed. Figure 18 also demonstrates that the grain size of the rim and core parts of the sample was similar.

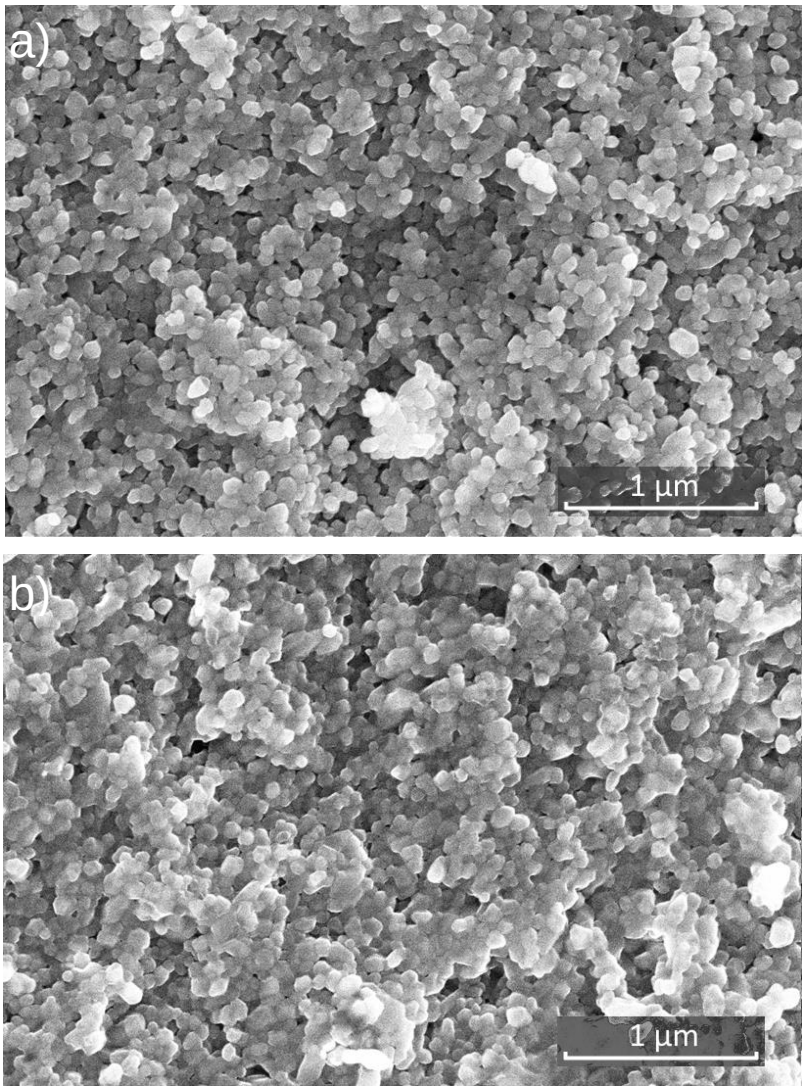

Figure 18. Sample ZnAc_30/3_05_1228 a) core (C area), b) rim (D area)

5.3 Soaking time – reaction time before the sintering

A Figure 19 shows the received relative density for samples with a different soaking time. Data were obtained for samples with an equal weight fracture of acetic acid solution (20 %wt) and a pressure level (50 MPa).

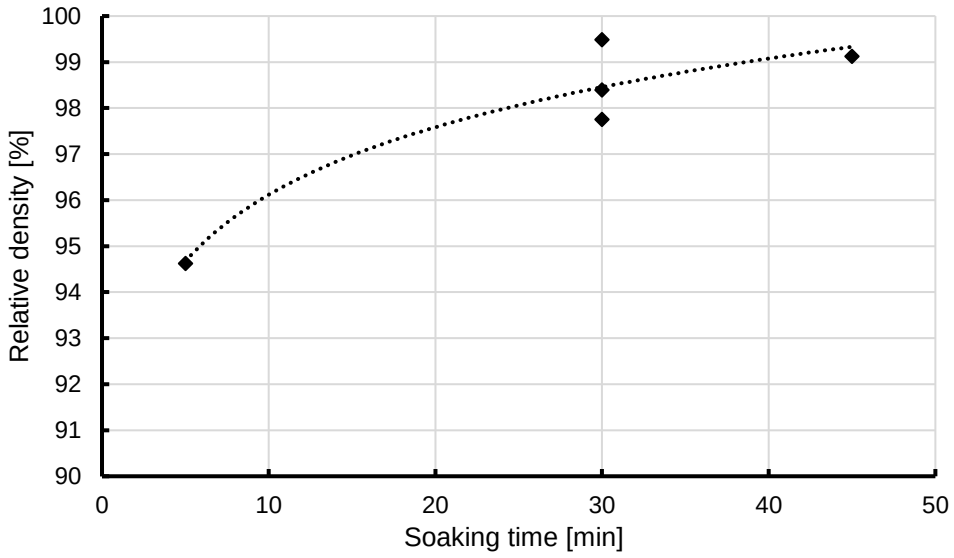

Figure 19 Time delay between mixing and sintering, ZnO samples with a 20 wt.% of 1 M aqueous solution of acetic acid, pressure 50 MPa

Together with a density, soaking time influenced the grain size. A sample ZnAc_30/1_05_1080 (Figure 20 a)) had a noticeable larger final grain size than a sample ZnAc_30/1_05_1079 (Figure 20 b)) which was – except the time of soaking – prepared by equivalent condition. These samples were prepared by low pressure (50 MPa).

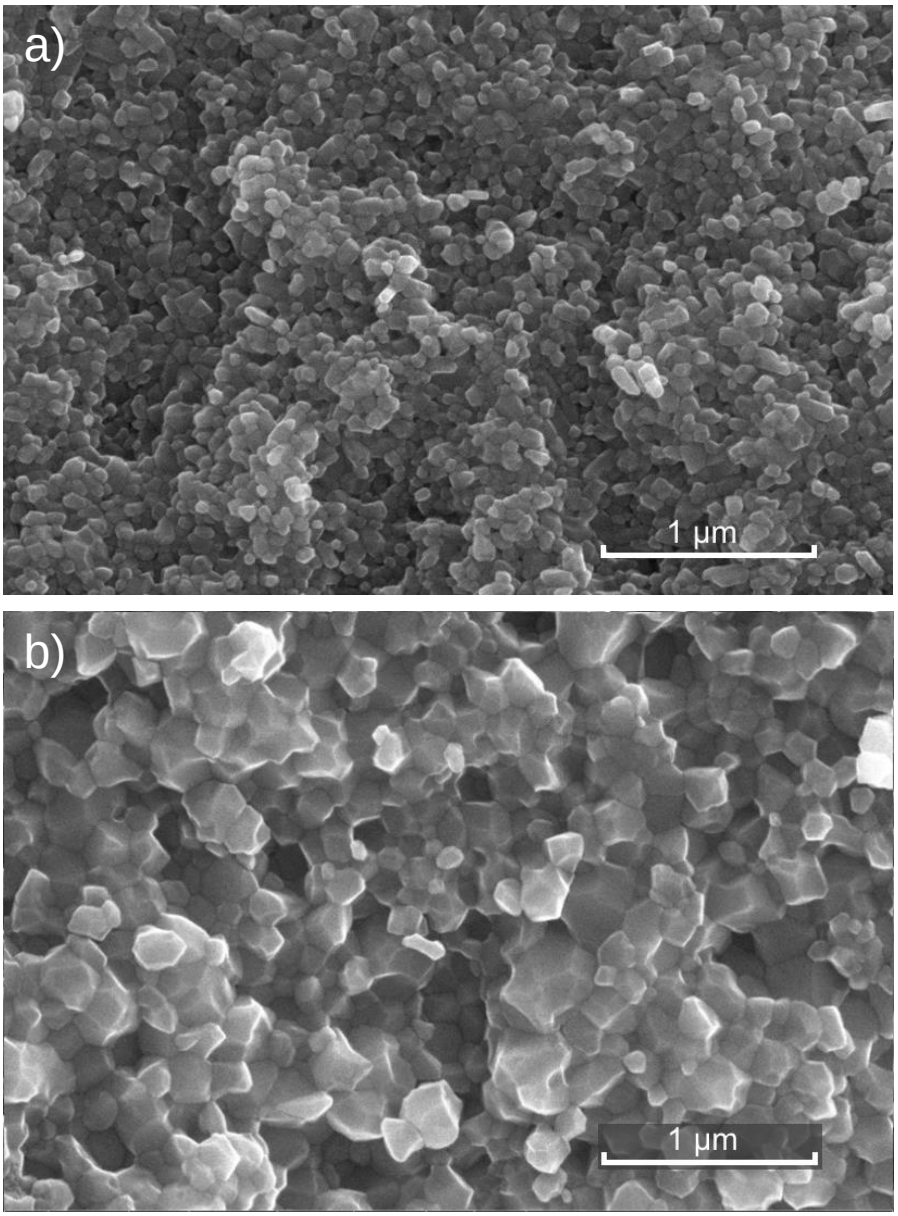

Figure 20 a) Sample with 5 minutes soaking time (ZnAc_30/1_05_1079) and b) with 30 minutes soaking time (ZnAc_30/1_05_1080) sintered at same conditions (50MPa and 300 °C)

5.4 Color and texture after CSP

An inhomogeneous coloring was observed when pre-pressed pellets were wetted by drop wetting and diffuse wetting. The samples wetted by stirring in the mortar have homogeneous color and texture depending on the final density and applied pressure.

The diffuse wetting leads to the core-rim structure described above. The relative density of a sample depended on how long the pellet was wetted. The sample ZnAc_30/3_05_1228 which was wetted for 2 hours had a final density of 84 % TD. However, sample ZnAc_30/3_05_1226, after twice of time of wetting, had a density of 90 % TD.

A “cloudy” texture (the Figure 21 b)) appeared if the sample was wetted by dropping indicating that the densification was not homogenous.

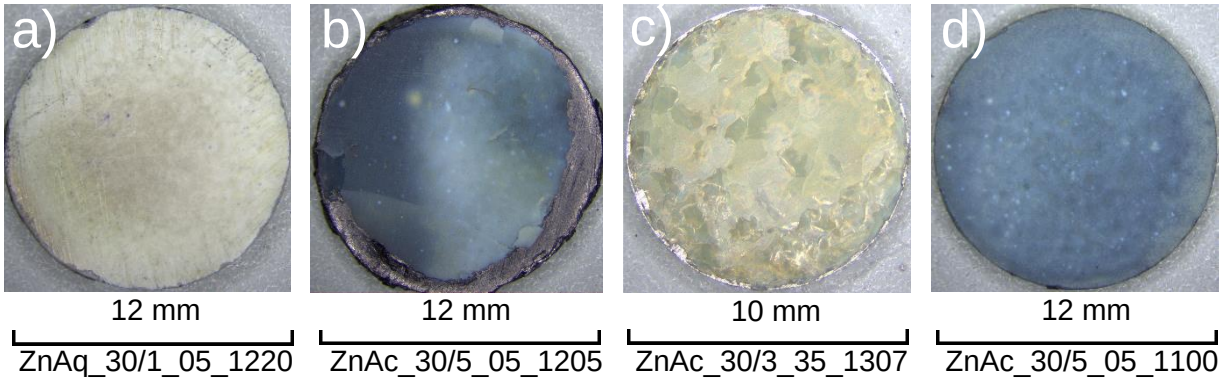

Figure 21 Samples prepared by cold sintering, a) In in the mortar with final density < 80 %, d) with final density 95 %, c) by high pressure, b) diffusion wetting (96 %)

In the Figure 21 there are examples of sample variability. The samples with a low density (below 80 %TD) had a white color figure a). The core-rim texture in the Figure 17 was a result of the sintering the diffusively wetted sample. Inhomogeneous distribution of a common for both diffusively and by drops wetted samples.

Generally, the higher level of pressure (300 MPa) caused that the sintered sample was translucent. The optical properties were related with a relative density however this effect did not appear in the case of 50 MPa samples.

The second parameter which significantly influences the color and texture of the sintered sample is the amount of the present liquid on the beginning. The higher amount of the starting solution (20 wt.%) promotes dark blue color instead of yellow color promoted by a low amount of solution (5 wt.%). The samples without a solution are white (and have low density), but if the water was not leaving the sintering chamber the mild blue color occurred (ZnAq_30/1_30_1257).

Table 4 Visual properties and wetting characteristics

Name	Wetting technique	Liquid content [wt.%]	Soaking time [min]	Relative density [%]	Visual properties
ZnAc_30/3_05_1226	Diffusion	24	240	90	Dark blue rim, blue core
ZnAc_30/3_05_1228	Diffusion	10	120	83	Blue green rim, white core
ZnAc_30/5_05_1205	Dropping	20	30	96	Blue/dark blue texture
ZnAc_30/3_35_1307	Standard	5	50	94	Yellow green, low translucency
ZnAc_30/3_30_1166	Standard	20	30	97	Blue green color, translucent
ZnAc_30/5_05_1100	Standard	20	30	98	Blue color with light dots
ZnAq_30/1_30_1257	Standard	20	“30”	-	Light blue color, homogenous
ZnAq_30/1_05_1220	Standard	10	“20”	79	White colour

The Table 4 Visual properties and wetting characteristicsTable 4 contains the visual properties and wetting conditions of selected samples. The apostrophes were used to distinguish the soaking in water from soaking in an acetic solvent because in the case of water reaction with a powder was unexpected. The relative density of a ZnAq_30/1_30_1257 is not listed. The sample was prepared in an aluminium foil which glued a sample with a die, so higher force was needed to extract the sample. In combination with a low mechanical property of the poorly sintered sample damaged the sample was obtained which was unfavorable for density measurement.

5.5 Temperature dependence

The final sintering temperature 180, 240, and 300 °C were used to demonstrate sintering behavior, see Figure 22. The final density of the ZnO samples increased with the final temperature. The increase in density was also observed by an SEM (see Figure 23).

The second examined sintering parameter was the heating rate to the sintering temperature of 300 °C, see the Figure 24. The achieved relative density was not dependent on a heating rate, because the values were similar.

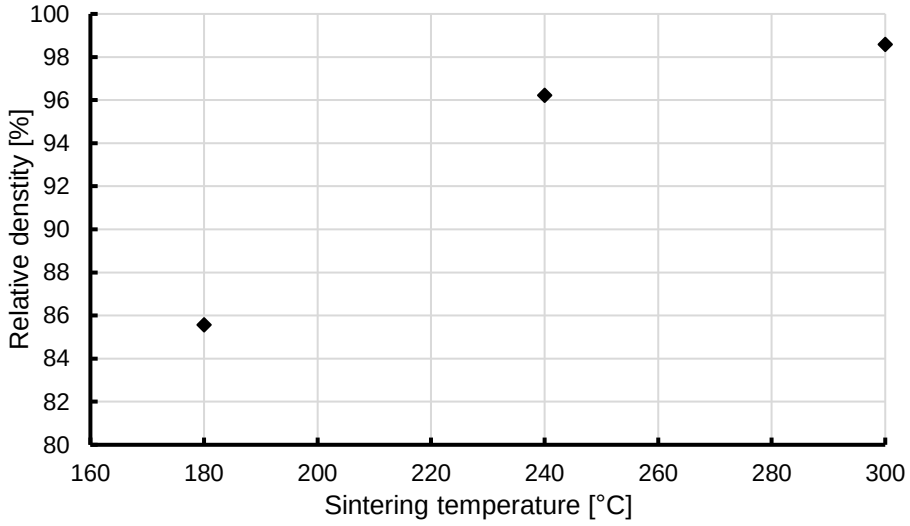

Figure 22 An effect of sintering temperature on a reached theoretical density, ZnO samples with a 20 wt.% of 1 M aqueous solution of acetic acid, pressure 50 MPa

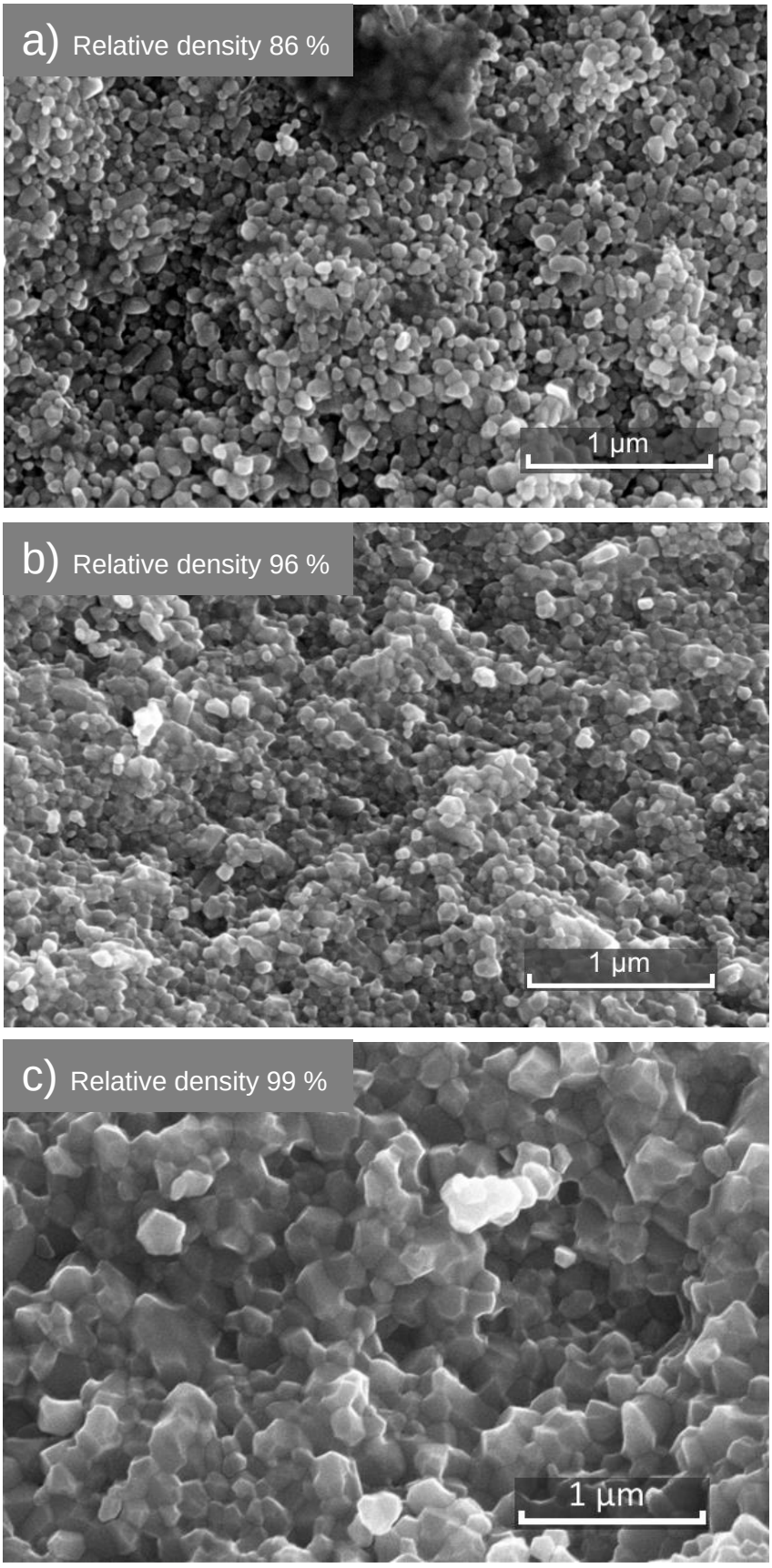

Figure 23 Sample sintered at different temperatures 180 °C, 240 °C, and 300 °C a) ZnAc_18/3_05_1199, b) ZnAc_24/3_05_1198, c) ZnAc_30/01_05_1080.

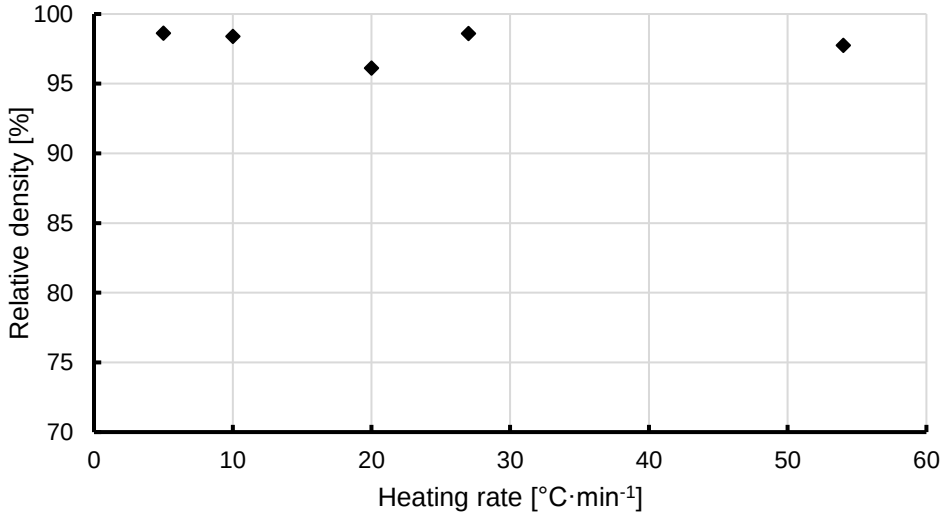

Figure 24 Theoretical density dependence on the heat rate: ZnO samples with a 1 M aqueous solution of acetic acid

5.6 Vapor escape

Characteristic peaks appeared in the development of effective gas pressure. Generally, two significant events appeared during sintering if a fraction of around 20 %wt of solvent was used. The Figure 25 is an example of the ordinary effective gas evolution.

The Figure 26 is the map of gas pressure peaks. For a clarity, peaks were divided by a threshold line of 130 °C (marked by dashes). Low temperature peaks appeared near a temperature of 100 °C. The span between low and high temperatures peaks is, for each sample, visualized by a black line. The span between high temperature peaks is visualized by a hatched line. The distance between peaks is relatively similar till a 50 °C·min^{-1} but with a different starting point.

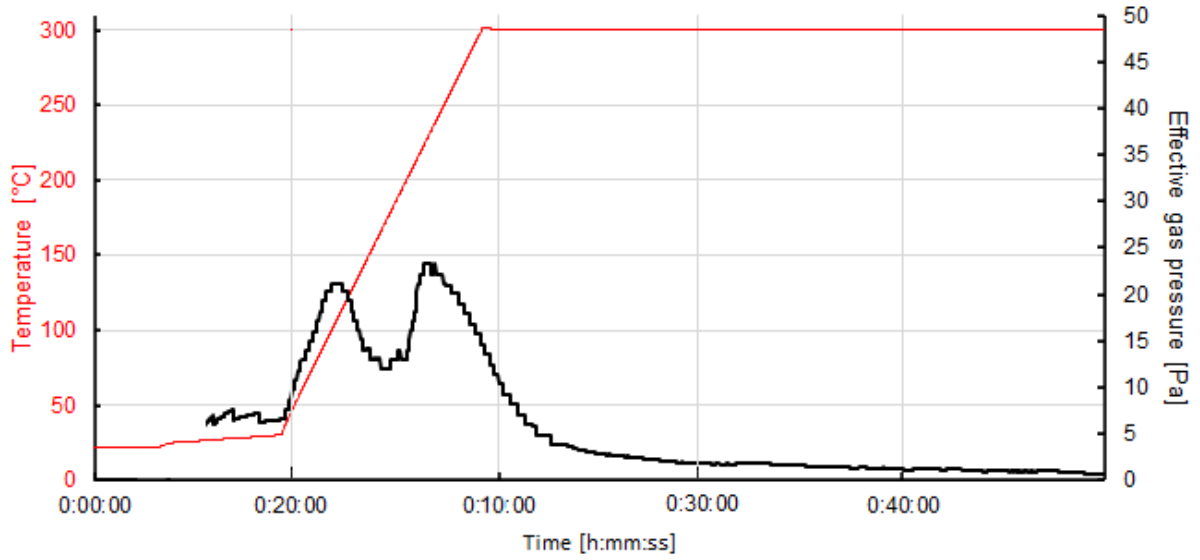

Figure 25 The temperature and effective gas evolution during sintering, ZnAc_30/3_05_1101

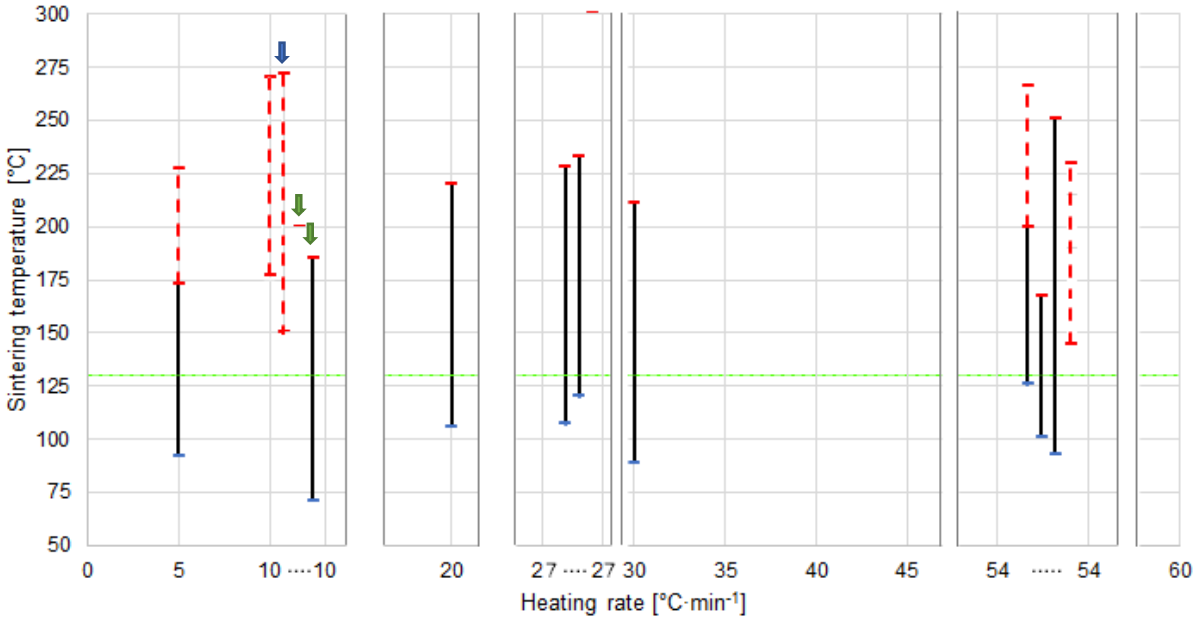

Figure 26 The map of peaks and the span between, the green line is the 130 °C threshold which divides peaks to low and (blue/red dash), the span between low and high-temperature peaks is visualized by a black line, the red hatched line is a span between high-temperature points. samples with 20 wt.% (except the one with 10 wt.% blue arrows) content of 1 M acetic acid, 50 MPa, green arow points out samples prepared by a short soaking time (~5 min)

Comparison of graphite and aluminium sealed sample

The leakage of the gas from the sintering die was also affected by the sealing of the sample. The graphite paper was used to seal the samples, but the quality of the sealing was questionable. Therefore, aluminium foil was used for the external sealing before the sample was inserted in a sintering die. Therefore, we can assume that gases are release at higher internal pressures, the sample ZnAq_30/10-60_1257 had no recorded gas leakage. Differences between applied pressures and the way sealing are demonstrated in Figure 27 and Figure 28, generally two peaks were observed, but at various temperatures and starting of the sintering, the procedure has also impact as well as the construction of the high-pressure die. Note that the high-pressure sintering use approximately half of the powder weight.

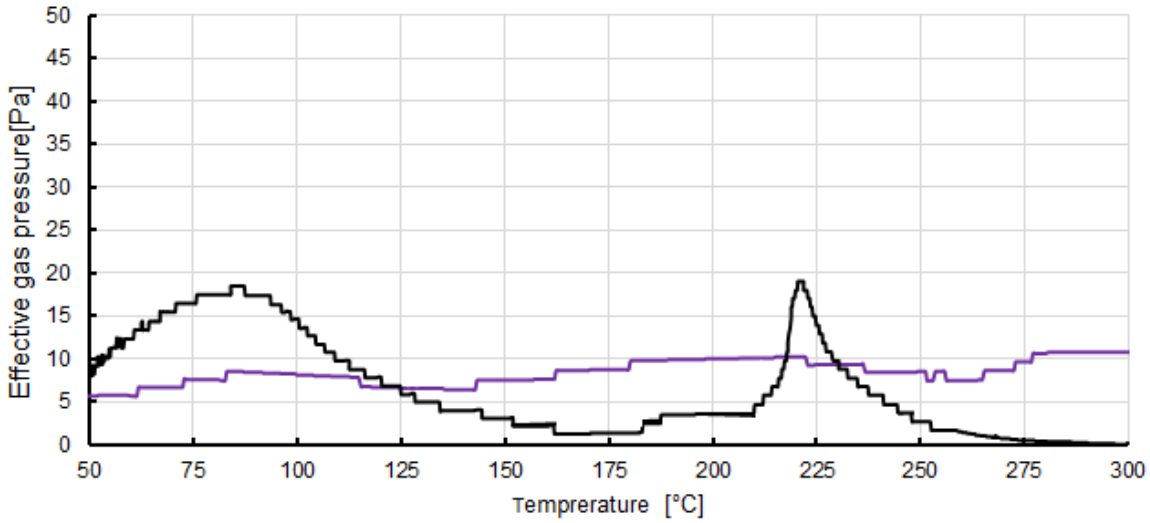

Figure 27, High-Pressure sintering: black curve sample without sealing (ZnAc_30/1_30_1165), purple curve sample with an aluminium sealing (ZnAc_30/3_30_1273)

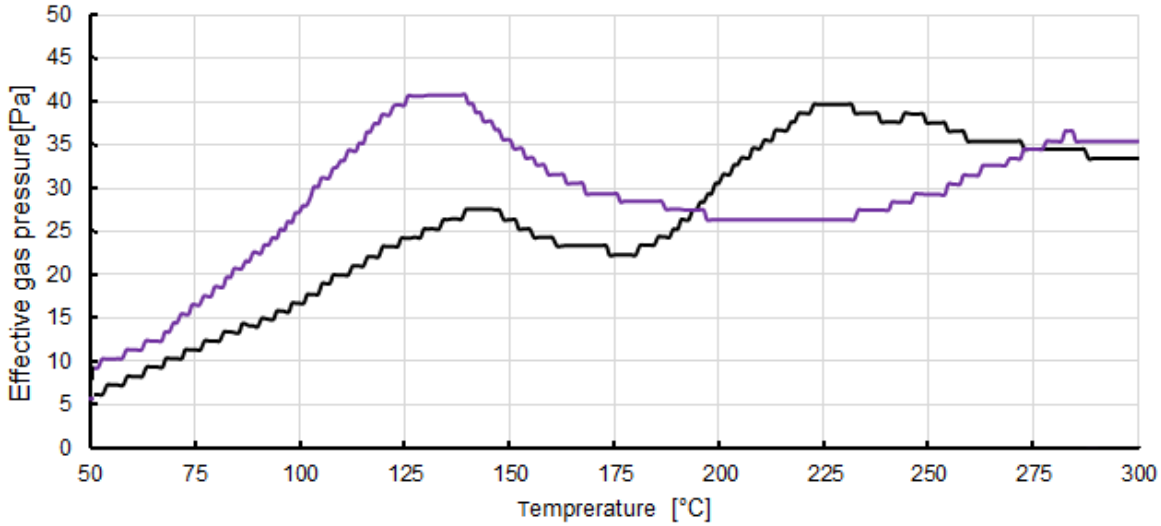

Figure 28 Low-pressure sintering: black curve sample with a graphite sealing (ZnAc_30/5_05_1207), purple curve sample with an aluminium sealing (ZnAc_30/5_05_1235)

5.7 Impact of high mechanical pressure

The leakage of a mixture around the punches happened already before the sintering procedure at room temperature (samples ZnAc_30/1_30_1160 and ZnAc_30/1_30_1165). Hence the measurement of dilatation was corrupted by high error.

Samples that were processed by high pressure (300 MPa) had a translucent property even the final density was not above 99 %. In the case of low pressed samples, translucency newer appeared.

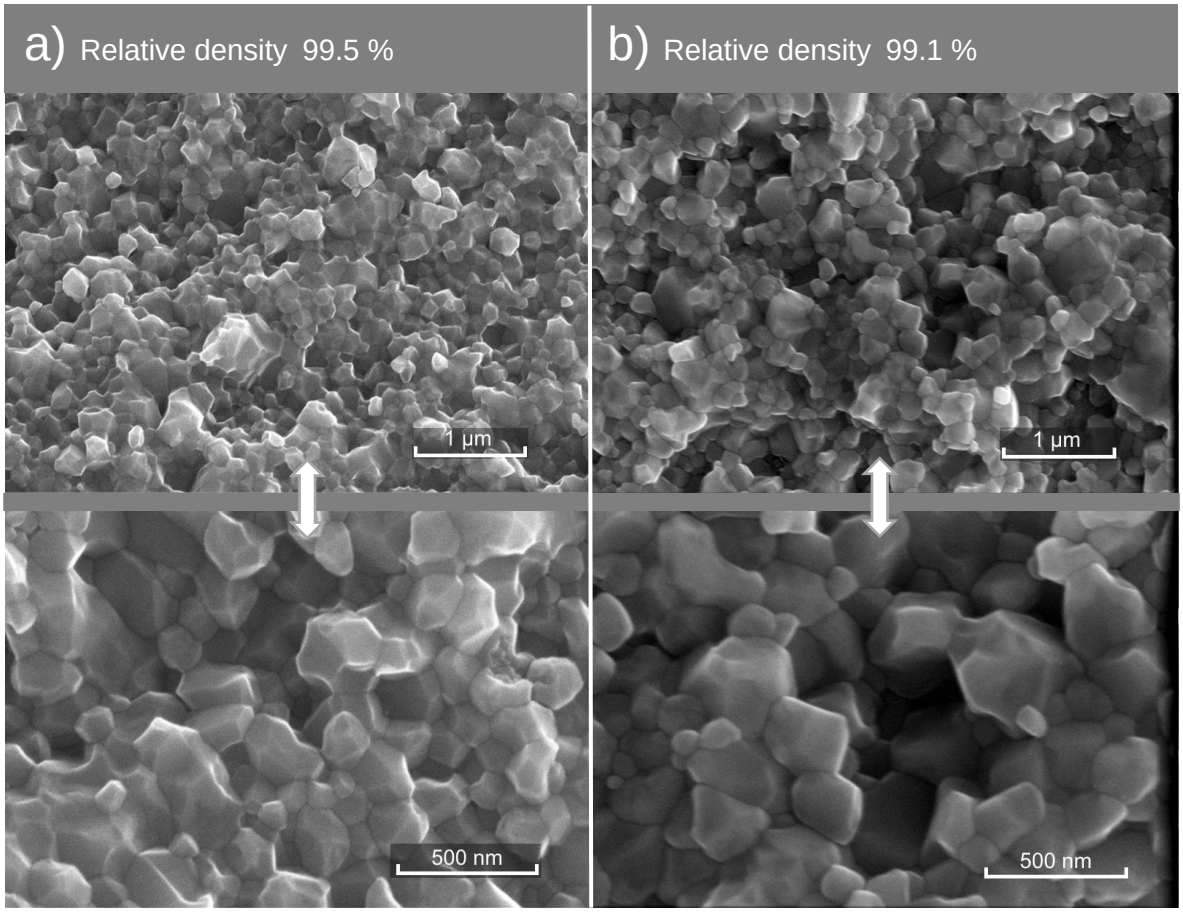

Figure 29 Pressure dependence on received density a) ZnAc_30/1_05_1080, b) ZnAc_30/1_30_1165

Grain size differences of sample ZnAc_30/1_05_1080 (99.5 TD) and ZnAc_30/1_30_1165 (99.1 TD) are small but higher pressure slightly promotes grain size as visible in the Figure 29.

Table 5 An effect of pressure, a solvent, and a sealing on a densification

Name	Maximal pressure [MPa]	Sealing	Solvent	Liquid content [wt.%]	Soaking time [min]	Relative density [%]
ZnAc_30/1_30_1160	300	-	AcOH	20	60	96
ZnAc_30/1_30_1165	300	-	AcOH	20	45	99
ZnAc_30/3_30_1166	300	-	AcOH	20	30	97
ZnAc_30/1_05_1070	50	Graphite	AcOH	20	30	98
ZnAc_30/3_30_1291	300	Aluminium	AcOH	20	45	69
ZnAc_30/3_30_1273	300	Aluminium	AcOH	20	45	95
ZnAc_30/3_35_1307	350	Aluminium	AcOH	05	50	94
ZnAc_30/5_05_1235	50	Aluminium	AcOH	20	30	94
ZnAq_30/1_30_1236	300	Aluminium	Aqua de.	15	“60”	-
ZnAq_30/1_30_1257	300	Aluminium	Aqua de.	20	“30”	-
ZnAq_30/1_05_1203	50	Graphite	Aqua de.	20	“30”	79

The Table 4 Visual properties and wetting characteristicsTable 5 contains pressure and solving wetting parameters for sintering. The apostrophes were used to distinguish the soaking in water from soaking in an acetic solvent. Relative density of a ZnAq_30/1_30_1257 and 1236 are not listed for the same reason as in Table 4 (see chapter 4.3).

5.8 Preliminary sintering of $BaTiO_3$

Sintering of $BaTiO_3$ nanopowder in DM water, acetic acid, and HCl solution did not lead to a densification of a ceramic. Almost no change of vacuum and displacement occurred if the hydrochloric acid was used. The microstructure of a barium titanate treated in acetic acid is visible in the Figure 30. The grain size of the processed powder is identical to a starting powder.

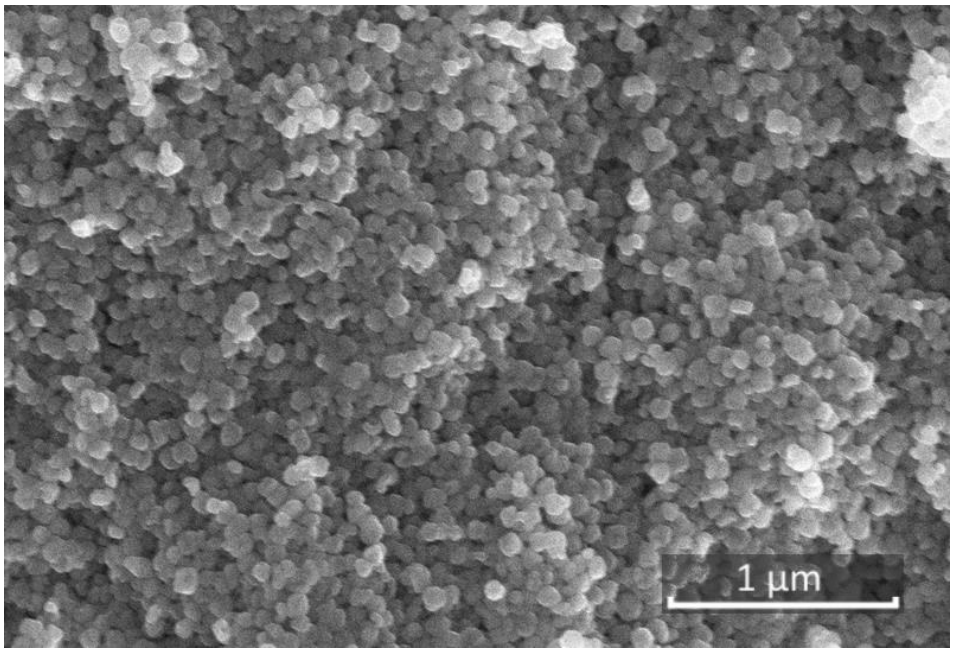

Figure 30, Low-pressure sintering of BaAc_30/3_05_1275, microstructure

6 DISCUSSION

6.1 Construction of the cold sintering die and sample loading

During a sintering problem with cracking of silicon carbide punches occurred (Figure 31). Therefore, they were changed for a punch made of a WC-Co. The cause of cracking was probably an eccentric loading as a result of cumulation of a geometric tolerance, plus the liquid inside the compacted powder could change a force distribution. Compare with the constructions demonstrated in the literature [12] SiC die was also used but reinforced because the addition of the liquid the transfer force on the inner cylinder can explain cylinder cracking (before the reinforcement). Because the inner force caused tension in a ceramic which the ceramic could not withstand. The application of WC-Co material was possible due to low temperatures. However, lower corrosion resistance is expected. Further development of the sintering dies as well as the loading procedure (including sealing) is expected.

Figure 31 Fracture surface of a SiC punch

6.2 Effect of a transient liquid – internal factors

Sintering was performed in a relatively high fraction of a liquid solution, similar to [45]. The higher content of a liquid was advantageous for a better vapor escape contemplation.

Although an original ZnO powder was white, samples prepared in a water solution had a blue or green color. With some exceptions shade of the color often said preliminary information if the relative density was high. The color change was observed for both demineralized water and acetic acid solvent. The blue-green color was caused by the presence of water during sintering. A research group Dargatz et al. 2016 [32] also reported a color change of ZnO samples when they were prepared in presence of water at a relatively low temperature of 400 °C. Research also reported a high hydrogen doping of these samples. If authors had increased the temperature to 800 °C, sintered discs had a yellow color. Another reason for the color change might be a presence of a structure disorder on a grain boundary or by a presence of impurities.

The poor wetting ability of a diffusive method and inhomogeneous densification was probably caused by the hydrophobicity of zinc oxide [45].

Soaking time

A dependence on the delay between sintering and powder mixing and a final density was observed. With a longer soaking time after mixing the ceramic has a greater density. This was probably caused by a chemical reaction between a powder and an acetic acid solution. The formation of zinc acetate was expected according to an Equation 1.

$$ZnO + 2CH_3COOH \rightarrow Zn(CH_3COO)_2 + H_2O \qquad (1)$$

More zinc acetate was expected to be formed in case of a longer dwell time between mixing and sintering due to the dissolution of zinc ions. The newly formed zinc acetate has higher thermal stability (200 – 350 °C) [42] than acetic acid. This can explain why after the short soaking time (time of the reaction between Zn and acetic acid) different shrinkage and final density was observed, see the Figure 32

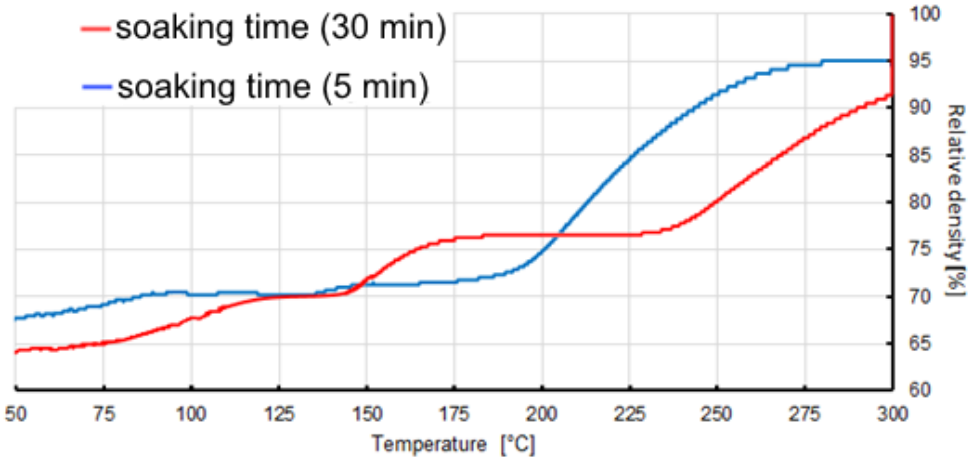

Figure 32 Comparison of a density dependence of samples prepared by 10 °C·min^{-1} and 50 MPa, prepared in a 20 %wt acetic acid solution with a different time they were left to stand after a wetting, red line ZnAc_30/1_05_1080, blue line ZnAc_30/1_05_1079

Another difference between samples with different soaking times is the densification at low temperature (Figure 32, below 50 °C) but it needs to be verified. Although the less reacted sample (soaking time 5 min) had a better starting point at 50 °C and reached higher relative density at beginning of the dwell time the final density was lower due to stagnation at dwell time.

6.3 Vapor escape effect on densification – internal factors

Pure water

Frequently a uniaxial press and heating jacket is used for cold sintering. In this case, an SPS device was used instead because of the adjustability and data output. The vacuuming of a chamber was used to protect a die against oxidation and to enable measurement of low changes in pressure due to a vapor escape. The same procedure was previously done by the Dargatz group (2016) to sinter a zinc oxide in a presence of water. The obtained development of an effective pressure is visible in the Figure 33.

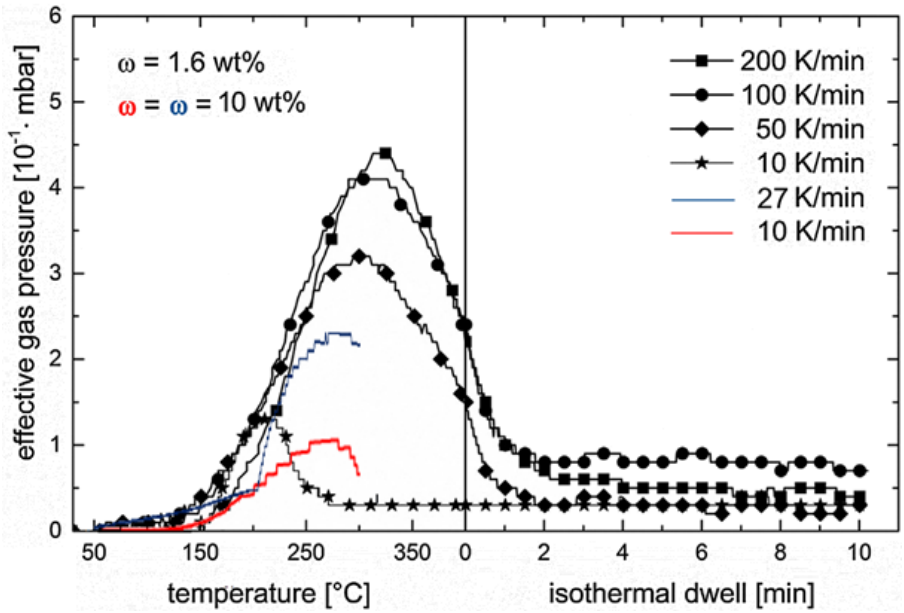

Figure 33 influence of a heating rate on development of vapor during sintering of the ZnO, DM water, original from a Benjamin Dargatz et al. (2016), black development was published by the author, blue and red data were obtained from a 12 mm die in contrast to a 20 mm die which was used by the group of Benjamin Dargatz [32]

The proportion between effective pressure measured by the Dargatz group (black curves) and the one obtained in the thesis is not correct. That is because author used a larger sintering form of 20 mm compared to a 12 mm form used in the thesis. As a result, the amount of an evaporated water seems to be similar in both experiments Figure 33. Pressure development of a 10 wt.% is showed till the temperature of 300 °C which was the maximal value for an experiment. A position of effective gas pressure peaks is comparable to a position reported by [32] for heating rates below 50 °C·min^{-1}. However, the maximal effective gas pressure of the sample sintered by 10 °C·min^{-1} (for the thesis – red line) is shifted to a higher temperature than the one observed by the Dargatz group. In both cases, graphite dies and pressure of 50 MPa was used for sintering. Hence the similar thermal properties are expected. The peak shift might be caused by a different tightness of dies or by different initial compactness of powders caused by a lower viscosity of a more wetted powder. It is also possible that more water needed more energy to be vaporized.

The maximal received relative density for water was 84 %, see Table 3 Comparison of sample densities, samples prepared by the same sintering temperature of 300 °C, pressure 50 MPa but with a different amount and type of transient liquid. The shrinking during a dwell time was minimal similar to sintering at a low soaking time in the solution, see previous chapter – 5.2 Soaking time. In the case of water, an increase in density started at 150–175 °C. Escape of water before this temperature had a non or neglectable effect on sintering (see the Figure 35, actual chapter, section Acetic acid solution).

Acetic acid solution

In the thesis constant pH was used since 1 M acetic acid was used for sintering. The concentration was selected concerning literature [16; 31; 30]. The pH of the 1 M solution is about 2.38. The pH is a crucial parameter of a reaction as was proved by several authors. It was previously observed that the pH condition suitable for cold sintering are outside the areas of precipitation [16]. The pH of pure water is on a breaking point of a precipitation curve (the Figure 34), which is the reason why the sintering in DM water was limited.

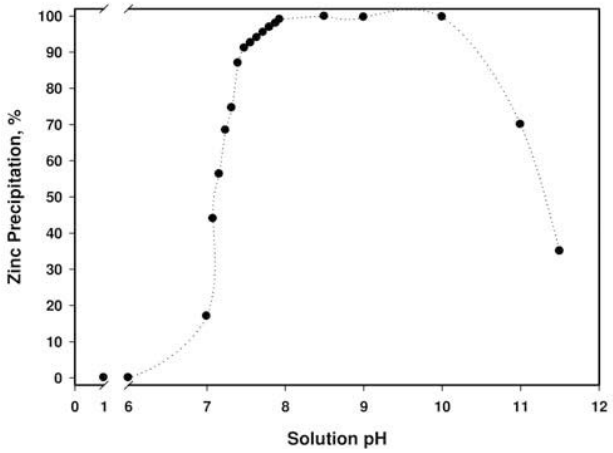

Figure 34 Zinc precipitation as a function of pH, from: [43]

In the Figure 35, a) the first peak, between 75–100 °C was caused by minor initial problems with temperature regulation, else the peak at low temperature (100 °C) was not observed (case of the sintering in water).

a) DM water

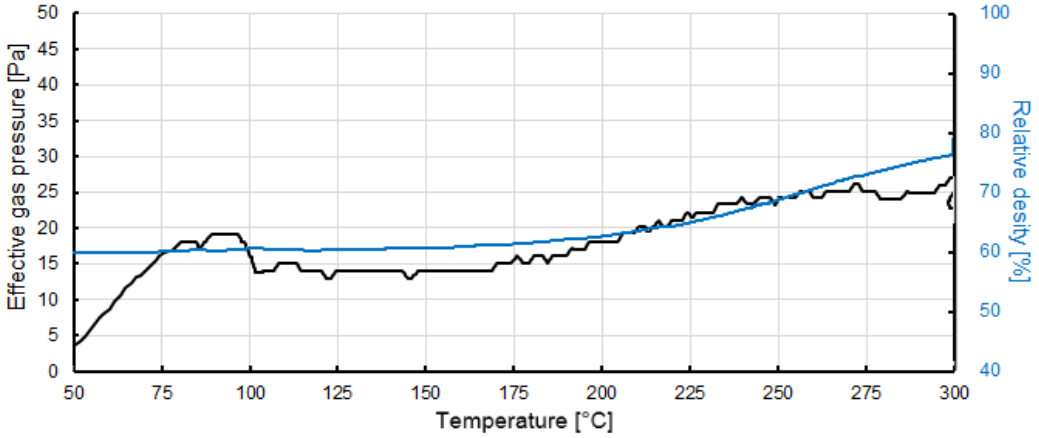

b) Acetic acid solution

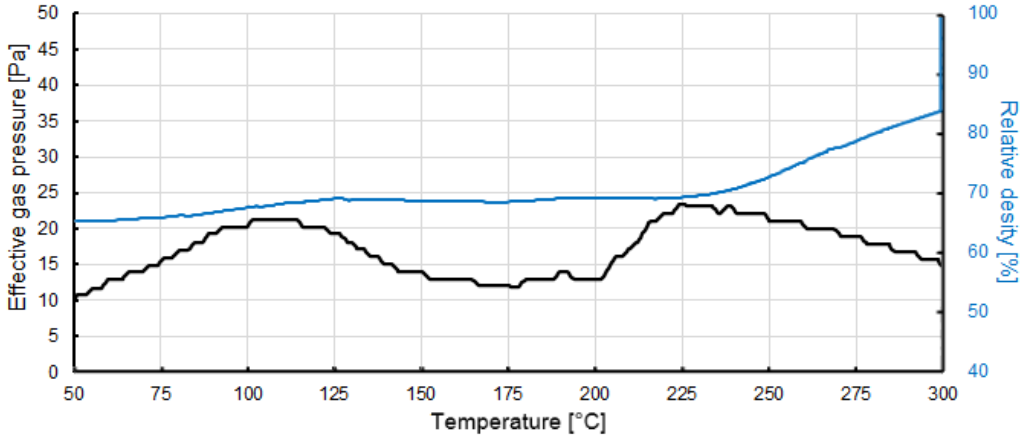

Figure 35 Comparison of a vapor escape and densification, a) sample ZnAq_30/3_05_1225 was sintered in a DM water, b) sample ZnAc_30/3_05_1101 was sintered in an acetic acid solution; both samples were made by equivalent sintering conditions: 300 °C, 27 °C·min^{-1}, 50 MPa

Generally, vapor development for an acetic acid contained two peaks. One appeared at a temperature of 100 °C which might suggest its origin is in the boiling point of water. The second peak appeared at a temperature of 200–250 °C. Two peaks can be partially explained by the decomposition of the zinc acetate, see the chapter 5.2, section – Soaking time. The decomposition of zinc acetate starts at a temperature of 200 °C but is not finally complete until 350 °C. Which might agree with the observation. [42]. The decomposition of a zinc hydroxide, which ordinally takes place at a temperature of 100 – 250 °C [44] is questionable. The reaction is possible however its contribution to effective gas pressure is expected to be low.

High-pressure die and sealing

The construction of the high pressure dies limits recording and sometimes even three peaks indication three released can appear, but this should be verified. Furthermore, the high-pressure die is using less solvent and therefore the vacuum drop is not so significant. This problem was amplified when

the aluminium sealing was used. Aluminum sealing was used to modify a gas escape. At this point, the aluminum was sealing too well so the escape of water was low leading to improper densification.

6.4 Sintering conditions – external factors

The effect of high-pressure sintering (above 50 MPa) is difficult to declare because samples with an almost theoretical density were possible to obtain at 50 MPa and the displacement curve was affected by leakage of a mixture. The application of high pressure was in many ways problematic. Apart from leaking the mixture with a low viscosity transferred the pressure on an inner face of a die and caused a rupture of a previous non-reinforced SiC die. Otherwise, the die would withstand more load if the powder was dry [12]. Therefore, the die was supported by a steel ring which compressed the die to reduce a tension caused by an inert pressure.

Translucent properties were observed for high-pressed samples (300 MPa). That would be proving of lower porosity of ceramic. The heating had a low but rather negative effect on densification. The reason was probably caused by a higher pressure of vapor, which acted against densification.

6.5 Preliminary sintering of $BaTiO_3$

Attempts to sinter a barium titanate in a solution of an acetic acid solution or a 35 % hydrochloric acid were not successful, because the ceramic passivated its surface. Hence the densification did not occur. This finding is in correspondence with a theory presented by Hanzheng Guo and Clive Randall [28]. Results confirmed that the reaction route is better for densification. The grain size of $BaTiO_3$ (see Figure 30) remains very similar to the 50 nm of the starting powder and only HCl solution enables the formation of the compact pellet. However, the density of the compacted pellet was only 60 % of the theoretical density.

The more promising route of $BaTiO_3$ sintering by CSP is the chemical reaction of TiO_2 and $Ba(OH)_2$ described in chapter: 2.4, section Barium titanate.

In literature, cold sintered $BaTiO_3$ was prepared at a temperature of 225 °C [34]. The cold Sintering process has a prerequisite to becoming a game-changing technology especially in the field of electronics. The proper adjustment of a sintering condition will be a serious task because of the complexity of a process but the mastering of the technology would decrease the cost of devices since the currently used noble metal would be substituted by a non-noble one.

7 CONCLUSIONS

The first part of the experiment in the thesis was focused on the preparation of a high-pressure die for a spark plasma sintering. The die was requested to be electrically conductive because of a pulse current that generates a Joule heat in the die and to be strong enough to resist high pressure. In the thesis double stage die was designed to fulfill these terms. The smaller-inner die was designed for high pressure, therefore it was made of silicon carbide because of mechanical properties of carbide and thermal properties, and excellent chemical durability. The durability of a die was further expanded when the inert die was reinforced by a steel ring. The thermal conductivity of a system was ensured by inserting the SiC die into a graphite die. The critical parts of the double stage die are SiC punches and SiC cylinders due to the tendency to crack. On the other hand, WC-Co inner die is mechanically stable and no significant corrosion was observed. Thus, the prepared die was successfully used to produce disks 10 mm in diameter by a pressure of 350 MPa at a temperature of 300 °C. Moreover, low pressure-die was successfully tested for the cold sintering process and disks with a diameter of 12 mm were produced.

Opportunities of the cold sintering process in the SPS apparatus were tested on ZnO powder, the influence of the sintering conditions, sample loading, and effect of vapor escape were examined. The SPS apparatus allowed recording of sintering data including the surrounding atmosphere (vacuum development and dilatation of a sample). The barometric measurement allowed detection of significant vapor escape during sintering and define the temperature of the escape, which advantage of the SPS apparatus. The observation of the sintering curve allowed to study of internal effects (sealing of a die, pH modulator, and its content) and the external factors (processing conditions – total temperature, heating rate, applied pressure). This brings new opportunities to compare with a conventional uniaxial pressing device.

The cold sintering process of ZnO powder demonstrated the possibility to receive high density up to 99.5 %TD at 300 °C and only 50 MPa by the addition of 20 wt. % of 1 M acetic acid. The analysis of the ZnO cold sintering process led to the following conclusions:

- From three methods of wetting techniques, the mechanical mixing (stirring) was chosen as the most appropriate because of the homogeneity of samples.
- The impact of reaction between powder and liquid – soaking time – was scoped in the thesis. The effect of soaking a ZnO powder in acetic acid was recognized as a positive for densification. The importance of soaking was identified as a result of a zinc acetate formation. A soaking time of 30 min was minimum to obtain the potential density. Because the zinc acetate is more thermally stable than the acetic acid causing that the pH modifier improved the sintering longer.

- The escape of vapor was proved to be important for proper densification as well as a fraction of transient liquid. A lot of liquid was harmful for densification if the sealing impeded it to escape.
- The change in the color of samples was registered. The change was a result of sintering in a presence of water. The shade of color changed with the water content and the color was duller/lighter if the density was high/low. With an increase of input water, the color changed from white/yellow (low amount of water or the densification did not occur) to green and blue.
- Almost theoretical density was achieved for both the pressure 50 MPa and 300 MPa. However, the application of high pressure was found to be problematic due to a viscosity of a mixture.

Preliminary tests of the $BaTiO_3$ cold sintering process demonstrated the only small impact of acetic solutions (acetic acid or hydrochloric acid). According to the literature review, reactive sintering is a more promising route for CSP of $BaTiO_3$.

LITERATURE

[1] MURR, Lawrence E. A Brief History of Metals. MURR, Lawrence E. *Handbook of Materials Structures, Properties, Processing and Performance* [online]. Cham: Springer International Publishing, 2015, s. 3-9 [cit. 2021-03-10]. ISBN 978-3-319-01814-0. Dostupné z: doi:10.1007/978-3-319-01815-7_1

[2] DURSUN, Sinan, Kosuke TSUJI, Sun Hwi BANG, Arnaud NDAYISHIMIYE a Clive A. RANDALL. A Route towards Fabrication of Functional Ceramic/Polymer Nanocomposite Devices Using the Cold Sintering Process. *ACS Applied Electronic Materials*. American Chemical Society, 2020, **2**(7), 1917-1924. Dostupné z: doi:10.1021/acsaelm.0c00225

[3] GUTMANAS, E.Y., A. RABINKIN a M. ROITBERG. Cold sintering under high pressure. *Scripta Metallurgica*. 1979, **13**(1), 11-15. ISSN 0036-9748. Dostupné z: doi:https://doi.org/10.1016/0036-9748(79)90380-6

[4] JIANG, Anna, Daoyao KE, Ludi XU, Qiang XU, Jiang LI, Jiabei WEI, Chunfeng HU a Salvatore GRASSO. Cold Hydrostatic Sintering: From shaping to 3D printing: From shaping to 3D printing. *Journal of Materiomics*. 2019, **5**(3), 496-501. ISSN 2352-8478. Dostupné z: doi:https://doi.org/10.1016/j.jmat.2019.02.009

[5] SPUSTA, Tomáš. *Study of transition from open to closed porosity stage during sintering of advanced ceramic materials*. Brno, 2015. Master thesis. Brno University of Technology, Faculty of mechanical engineering, Institute of material science and engineering. Vedoucí práce Karel Maca.

[6] RAHAMAN, M.N. *Ceramic processing and sintering* [online]. 2nd ed. New York: Marcel Dekker, 2003 [cit. 2021-05-19]. Materials engineering. ISBN 08-247-0988-8. Dostupné z: https://www.academia.edu/5600888/Ceramic_Processing_and_Sintering_Rahaman_PDF

[7] GERMAN, Randall M., Pavan SURI a Seong Jin PARK. Review: liquid phase sintering: liquid phase sintering. *Journal of Materials Science*. 2009, **44**(1), 1-39. ISSN 1573-4803. Dostupné z: doi:10.1007/s10853-008-3008-0

[8] LEE, Sang-Ho, Elizabeth R. KUPP, Adam J. STEVENSON et al. Hot Isostatic Pressing of Transparent Nd: YAG Ceramics. *Journal of the American Ceramic Society* [online]. 2009, **92**(7),

1456-1463 [cit. 2021-04-18]. ISSN 00027820. Dostupné z: doi:10.1111/j.1551-2916.2009.03029.x

[9] *Ceramic Materials* [online]. 2nd. New York, NY: Springer New York, 2007 [cit. 2021-04-17]. ISBN 978-0-387-46270-7. Dostupné z: doi:10.1007/978-0-387-46271-4

[10] CINERT, Jakub. *Study of mechanisms of the Spark Plasma Sintering technique*. Prague, 2018. Doctoral thesis. Czech Technical University in Prague, FEE. Vedoucí práce Bouda, Václav.

[11] HUGHES, Lauren A. a Klaus VAN BENTHEM. Spark Plasma Sintering Apparatus Used for the Formation of Strontium Titanate Bicrystals. *Journal of Visualized Experiments* [online]. Department of Materials Science and Engineering, University of California, Davis, 2017, **2017**(120) [cit. 2021-04-29]. ISSN 1940-087X. Dostupné z: doi:10.3791/55223

[12] SOKOL, M., S. KALABUKHOV, M.P. DARIEL a N. FRAGE. High-pressure spark plasma sintering (SPS) of transparent polycrystalline magnesium aluminate spinel (PMAS). *Journal of the European Ceramic Society* [online]. 2014, **34**(16), 4305-4310 [cit. 2021-04-04]. ISSN 09552219. Dostupné z: doi:10.1016/j.jeurceramsoc.2014.07.022

[13] BALIMA, Felix, Oudomsack VIRAPHONG a Alain LARGETEAU. HP-SPS at very high pressure (6 GPa) for hard and super hard materials. *International Workshop on Spark Plasma Sintering*. Cagliary, Italy: Univ. Bordeaux, 2018, **4**(23-25), 2.

[14] GRASSO, Salvatore, Hidehiro YOSHIDA, Harshit PORWAL, Yoshio SAKKA a Mike REECE. Highly transparent α-alumina obtained by low cost high pressure SPS. *Ceramics International* [online]. 2013, **39**(3), 3243-3248 [cit. 2021-04-18]. ISSN 02728842. Dostupné z: doi:10.1016/j.ceramint.2012.10.012

[15] GUILLON, Olivier, Jesus GONZALEZ-JULIAN, Benjamin DARGATZ, Tobias KESSEL, Gabi SCHIERNING, Jan RÄTHEL a Mathias HERRMANN. Field-Assisted Sintering Technology/Spark Plasma Sintering: Mechanisms, Materials, and Technology Developments. *Advanced Engineering Materials* [online]. 2014, **16**(7), 830-849 [cit. 2021-04-18]. ISSN 1438-1656. Dostupné z: doi:10.1002/adem.201300409

[16] BEALL, T. M. *Cold Sintering of Ceramics*. Delft University of Technology, 2017. Dostupné také z: https://repository.tudelft.nl/islandora/object/uuid:8f07b5bf-27ee-467b-8c89-cb79fa748669/datastream/OBJ/download. Master thesis. Delft University of Technology, TU Delft Aerospace Engineering; TU Delft Aerospace Structures & Materials. Vedoucí práce Prof. Dr.W.A. Groen.

[17] BYRAPPA, Kullaiah a Masahiro YOSHIMURA. *Handbook of Hydrothermal Technology - A Technology for Crystal Growth and Materials Processing*. 2001.

[18] HIRANO, SHIN-ICHI a SHIGEYUKI SOMIYA. Hydrothermal Reaction Sintering of Pure Cr2O3. *Journal of the American Ceramic Society* [online]. 1976, **59**(11-12), 534-534 [cit. 2021-04-18]. ISSN 0002-7820. Dostupné z: doi:10.1111/j.1151-2916.1976.tb09432.x

[19] GRASSO, Salvatore, Mattia BIESUZ, Luca ZOLI, Gianmarco TAVERI, Andrew I. DUFF, Daoyao KE, Anna JIANG a Michael J. REECE. A review of cold sintering processes. *Advances in Applied Ceramics* [online]. 2020, **119**(3), 115-143 [cit. 2021-04-06]. ISSN 1743-6753. Dostupné z: doi:10.1080/17436753.2019.1706825

[20] NDAYISHIMIYE, Arnaud, Mert Y. SENGUL, Sun Hwi BANG et al. Comparing hydrothermal sintering and cold sintering process: Mechanisms, microstructure, kinetics and chemistry. *Journal of the European Ceramic Society* [online]. 2020, **40**(4), 1312-1324 [cit. 2021-02-23]. ISSN 09552219. Dostupné z: doi:10.1016/j.jeurceramsoc.2019.11.049

[21] *COLD SINTERING CERAMICS AND COMPOSITES*. 2016. United States. US20170088471A1. Uděleno 2020-08-04. Zapsáno 2016-09-27.

[22] WANG, Dixiong. *Low temperature processing of electro-ceramic materials and devices*. Pennsylvania, United States of America, 2020. A Dissertation. The Pennsylvania State University.

[23] ABRAHAMS, S.C. a K. NASSAU. Ferroelectric Materials. *Concise Encyclopedia of Advanced Ceramic Materials* [online]. 1. UK: Elsevier, 1991, s. 152-155 [cit. 2021-04-29]. ISBN 9780080347202. Dostupné z: doi:10.1016/B978-0-08-034720-2.50048-4

[24] VAKIFAHMETOGLU, Cekdar a Levent KARACASULU. Cold sintering of ceramics and glasses: A review. *Current Opinion in Solid State and Materials Science* [online]. 2020, **24**(1) [cit. 2021-02-19]. ISSN 13590286. Dostupné z: doi:10.1016/j.cossms.2020.100807

[25] NDAYISHIMIYE, Arnaud, Mert Y. SENGUL, Takao SADA et al. Roadmap for densification in cold sintering: Chemical pathways. *Open Ceramics* [online]. 2020, **2**(100019) [cit. 2021-04-13]. ISSN 26665395. Dostupné z: doi:10.1016/j.oceram.2020.100019

[26] ANDREWS, Jessica, Daniel BUTTON a Ian M. REANEY. Advances in Cold Sintering: Improving energy consumption and unlocking new potential in component manufacturing. *Johnson Matthey Technology Review* [online]. 2020, **64**(2), 219-232 [cit. 2021-04-04]. ISSN 2056-5135. Dostupné z: doi:10.1595/205651320X15814150061554

[27] TSUJI, Kosuke, Arnaud NDAYISHIMIYE, Sarah LOWUM, Richard FLOYD, Ke WANG, Maxwell WETHERINGTON, Jon-Paul MARIA a Clive A. RANDALL. Single step densification of high permittivity BaTiO3 ceramics at 300 ºC. *Journal of the European Ceramic Society* [online]. 2020, **40**(4), 1280-1284 [cit. 2021-04-01]. ISSN 09552219. Dostupné z: doi:10.1016/j.jeurceramsoc.2019.12.022

[28] GUO, Jing, Richard FLOYD, Sarah LOWUM, Jon-Paul MARIA, Thomas HERISSON DE BEAUVOIR, Joo-Hwan SEO a Clive A. RANDALL. Cold Sintering: Progress, Challenges, and Future Opportunities. *Annual Review of Materials Research* [online]. 2019, **49**(1), 275-295 [cit. 2021-02-19]. ISSN 1531-7331. Dostupné z: doi:10.1146/annurev-matsci-070218-010041

[29] GUO, Hanzheng, Amanda BAKER, Jing GUO, Clive A. RANDALL a D. JOHNSON. Cold Sintering Process: A Novel Technique for Low-Temperature Ceramic Processing of Ferroelectrics. *Journal of the American Ceramic Society* [online]. 2016, **99**(11), 3489-3507 [cit. 2021-04-01]. ISSN 00027820. Dostupné z: doi:10.1111/jace.14554

[30] FUNAHASHI, Shuichi, Jing GUO, Hanzheng GUO, Ke WANG, Amanda BAKER, Kosuke SHIRATSUYU a Clive RANDALL. Demonstration of the Cold Sintering Process Study for the Densification and Grain Growth of ZnO Ceramics. *Journal of the American Ceramic Society*. 2016, **100**. Dostupné z: doi:10.1111/jace.14617

[31] KANG, Xiaoyu, Richard FLOYD, Sarah LOWUM, Matthew CABRAL, Elizabeth DICKEY a Jon-Paul MARIA. Mechanism studies of hydrothermal cold sintering of zinc oxide at near room temperature. *Journal of the American Ceramic Society* [online]. 2019, **102**(8), 4459-4469 [cit. 2021-04-02]. ISSN 0002-7820. Dostupné z: doi:10.1111/jace.16340

[32] DARGATZ, Benjamin, Jesus GONZALEZ-JULIAN, Martin BRAM et al. FAST/SPS sintering of nanocrystalline zinc oxide—Part I: Enhanced densification and formation of hydrogen-related defects in presence of adsorbed water. *Journal of the European Ceramic Society* [online]. 2016, **36**(5), 1207-1220 [cit. 2021-04-02]. ISSN 09552219. Dostupné z: doi:10.1016/j.jeurceramsoc.2015.12.009

[33] LOWUM, Sarah, Richard FLOYD, Raul BERMEJO a Jon-Paul MARIA. Mechanical strength of cold-sintered zinc oxide under biaxial bending. *Journal of Materials Science* [online]. 2019, **54**(6), 4518-4522 [cit. 2021-04-02]. ISSN 0022-2461. Dostupné z: doi:10.1007/s10853-018-3173-8

[34] SADA, Takao, Kosuke TSUJI, Arnaud NDAYISHIMIYE, Zhongming FAN, Yoshihiro FUJIOKA a Clive A. RANDALL. Enhanced high permittivity BaTiO 3 –polymer nanocomposites

from the cold sintering process. *Journal of Applied Physics* [online]. 2020, **128**(8), 1-9 [cit. 2021-04-01]. ISSN 0021-8979. Dostupné z: doi:10.1063/5.0021040

[35] SADA, Takao, Zhongming FAN, Arnaud NDAYISHIMIYE, Kosuke TSUJI, Sun Hwi BANG, Yoshihiro FUJIOKA a Clive A. RANDALL. In situ doping of BaTiO 3 and visualization of pressure solution in flux-assisted cold sintering. *Journal of the American Ceramic Society* [online]. 2021, **104**(1), 96-104 [cit. 2021-04-01]. ISSN 0002-7820. Dostupné z: doi:10.1111/jace.17461

[36] Properties and characteristics of graphite. *POCO GRAPHITE An Entegris company* [online]. 2015, **2015**, 42 [cit. 2021-04-15]. Dostupné z: www.poco.com

[37] RICHTER, Janusz a Rafał MICHALIK. Corrosion resistance of WC-Co and WC-Ni type sintered carbides in acetic acid water solution. *Materials and Corrosion* [online]. 2019, **70**(1), 128-134 [cit. 2021-05-14]. ISSN 09475117. Dostupné z: doi:10.1002/maco.201810300

[38] SPARK PLASMA SINTERING – SPS: HIGH PERFORMANCE SOLUTIONS. In: *Mersen group* [online]. Courbevoie, France: Mersen, s. 2 [cit. 2021-05-19]. Dostupné z: https://www.mersen.com/products/graphite-specialties/isostatic-graphite-and-extruded-graphite/sintering

[39] Make Welding Processes Efficient with Silicon Nitride Ceramics. *Ceramtec* [online]. CeramTec-Platz 1-9 73207 Plochingen Germany: © CeramTec GmbH, 2021 [cit. 2021-05-19]. Dostupné z: https://www.ceramtec.com/competence/welding-technology/?gclid=EAIaIQobChMIjqmrkfLV8AIVjeR3Ch2V-AH4EAAYASAAEgLcDfD_BwE

[40] *ROCAR® Silicon Carbide: Special Materials for Machines and Devices* [online]. In: . Šumperk, Czech Republinc: CeramTec Czech Republic, s.r.o., s. 16 [cit. 2021-05-19]. Dostupné z: https://www.ceramtec.com/files/cz_rocar_en.pdf

[41] Tungsten Carbide - An Overview. *Azo materials* [online]. Manchester, UK: AZoNetwork UK Ltd. [cit. 2021-05-19]. Dostupné z: https://www.azom.com/properties.aspx?ArticleID=1203

[42] JIANG, Xupeng, Guisheng ZHU, Huarui XU et al. Preparation of high density ZnO ceramics by the Cold Sintering Process. *Ceramics International* [online]. 2019, **45**(14), 17382-17386 [cit. 2021-05-21]. ISSN 02728842. Dostupné z: doi:10.1016/j.ceramint.2019.05.298

[43] SUBEDI, Deepak Prasad, Dinesh Kumar MADHUP, Ashish SHARMA, Ujjwal Man JOSHI a Andrzej HUCZKO. Retracted: Study of the wettability of ZnO nanofilms. *International Nano*

Letters [online]. 2012, **2**(1), 1-4 [cit. 2021-04-19]. ISSN 2008-9295. Dostupné z: doi:10.1186/2228-5326-2-1

[44] MAR, G. L., P. Y. TIMBRELL a R. N. LAMB. Formation of Zinc Oxide Thin Films by the Thermal Decomposition of Zinc Acetate. HOWE, Russel F., Robert N. LAMB a Klaus WANDELT, ed. *Surface Science* [online]. 1. Berlin, Heidelberg: Springer Berlin Heidelberg, 1993, s. 177-192 [cit. 2021-04-20]. Springer Proceedings in Physics. ISBN 978-3-642-84935-0. Dostupné z: doi:10.1007/978-3-642-84933-6_15

[45] AKTAS, S. a M. H. MORCALI. Recovery of mercury from spent silver oxide button cells. *Mining, Metallurgy & Exploration* [online]. 2011, **28**(4), 198-203 [cit. 2021-05-12]. ISSN 2524-3462. Dostupné z: doi:10.1007/BF03402452

[46] WANG, Mingsong, Yajun ZHOU, Yiping ZHANG, Sung Hong HAHN a Eui Jung KIM. From Zn(OH)2 to ZnO: a study on the mechanism of phase transformation. *CrystEngComm* [online]. 2011, **13**(20), 13 [cit. 2021-04-02]. ISSN 1466-8033. Dostupné z: doi:10.1039/c1ce05502j

LIST OF TABLES

LIST OF FIGURES

APPENDIX

Calculations for the cylinder assembly

Preliminary calculations were made to estimate the overlap of a reinforcing steel ring and the central die. The first geometric parameter of the shaft/ring and bolt/die was calculated according to Equation 2 and 3.

$$G_B = \frac{d_B^2 + d_S^2}{d_B^2 - d_S^2} \qquad (2)$$

$$G_S = \frac{d_S^2 + d_H^2}{d_S^2 - d_H^2} \qquad (3)$$

Where the d_B represents the diameter of a bolt/die, d_S – diameter of shaft/ring, and d_H is the diameter of the central hole.

$$G_B = \frac{49.84^2 + 40.05^2}{49.84^2 - 40.05^2} = 4.65\ [-]$$

$$G_S = \frac{40.05^2 + 10.00^2}{40.05^2 - 10.00^2} = 1.14\ [-]$$

The value of overlapping was calculated by equation 3.

$$\Delta d = p \cdot d_S \cdot \left[\frac{G_B + \mu_B}{E_B} + \frac{G_S + \mu_S}{E_S}\right] \qquad (4)$$

Where p represents radial pressure, E_B and E_S the is young modulus and the μ_B and μ_S are poison rations of the bolt and the shaft.

The requested overlapping was calculated to generate a radial pressure of 150 MPa. The material constants are visible below.

E_S = 210,000 MPa

E_B = 410,000 MPa

μS = 0.33

μB = 0.16

$$\Delta d = 150 \cdot 40.05 \cdot \left[\frac{4.65 + 0.16}{410{,}000} + \frac{1.13 + 0.33}{210{,}000}\right] = 0.16\ mm$$

The overlap of a steel ring and vessel was estimated as 0.16 mm.

Temperature of assembly

α_{SiC} = $4.1 \cdot 10^{-6}$ K^{-1}

$L_{0,\,SiC}$ = 40.21 mm

α_{Steel} = 16·10^{-6} K^{-1}

$L_{0,\,Steel}$ = 40.05 mm

The convenient backlash for the assembly was estimated to be 100 μm. Temperature for the assembly was predicted using Equation 5.

$$L = L_0(1 + \alpha \cdot \Delta T) \qquad (5)$$

$$L_{SiC} - L_{Steel} = -0.10$$

$$L_{SiC} = L_{0,SiC}(1 + \alpha_{SiC} \cdot \Delta T);\ L_{Steel} = L_{0,Steel}(1 + \alpha_{Steel} \cdot \Delta T)$$

$$L_{0,SiC} + L_{0,SiC} \cdot \alpha_{SiC} \cdot \Delta T - L_{0,Steel} - L_{0,Steel} \cdot \alpha_{Steel} \cdot \Delta T = -0.10$$

$$\Delta T \cdot \left(L_{0,SiC} \cdot \alpha_{SiC} - L_{0,Steel} \cdot \alpha_{Steel}\right) = -0.10 - L_{0,SiC} + L_{0,Steel}$$

$$\Delta T = \frac{-0.10 - L_{0,SiC} + L_{0,Steel}}{\left(L_{0,SiC} \cdot \alpha_{SiC} - L_{0,Steel} \cdot \alpha_{Steel}\right)}$$

$$\Delta T = \frac{-0.10 - 40.21 + 40.05}{(40.21 \cdot 4.1 \cdot 10^{-6} - 40.05 \cdot 16 \cdot 10^{-6})}$$

$$\Delta T = \frac{-0.10 - 40.21 + 40.05}{(40.21 \cdot 4.1 \cdot 10^{-6} - 40.05 \cdot 16 \cdot 10^{-6})} = 546\ ^{\circ}C$$

LIST OF ABBREVIATION AND SYMBOLS

Abbreviations

AcOH	Acetic acid
CFC	Carbon fibre composite
CSP	Cold sintering process
DM	Demineralized (water)
FET	Field-effect transistor
FIB	Focused ion beam
HHP	Hydrothermal hot pressing
HRS	Hydrothermal reaction sintering
HS	Hydrostatic sintering
LPS	Liquid phase sintering
LPS	Liquid phase sintering
PTFE	Polytetrafluoroethylene
rHLPS	Hydrothermal liquid-phase densification
SAW	Surface acoustic wave
SEM	Scanning electron microscopy
SPS	Spark plasma sintering

List of Symbols

TD	Theoretical density	[g·cm^{-3}]
γ^{SG}	Interfacial solid/gas energy	[J·m^{-2}]
γ^{SS}	Interfacial solid/solid energy [J·m^{-2}]	[J·m^{-2}]
A	Surface area	[m^2]
σ	Stress	[N·m^{-1}]
γ	Surface energy	[J·m^{-2}]
r	Radii of arc	[m]
R	Radii of particle	[m]
m_f	Final mass	[kg]
h_f	Final height	[kg]
ϱ_f	Final relative density	[%]
ϱ	Relative density	[%]
A_i	Initial surface area	[m^2]
h_i	Initial height	[m]
h	Height	[m]
m_A	Weight of sample in air	[kg]
m_L	Weight of sample in auxiliary liquid	[kg]
ϱ_L	The theoretical density of liquid	[g·cm^{-3}]
ϱ_A	Theoretical density of air	[g·cm^{-3}]

G_B	Geometric parameter of bolt	[-]
G_S	Geometric parameter of shaft	[-]
d_B	diemeter of bolt	[m]
d_S	diemeter of shaft	[m]
d_H	diemeter of hole	[m]
p	Pressure (radial)	[$N \cdot m^{-1}$]
Δd	Overlapping	[m]
μ_s	Poison ration of shaft	[-]
μ_B	Poison ration of bolt	[-]
E_S	Young's modulus of shaft	[$N \cdot m^{-1}$]
E_B	Young's modulus of bolt	[$N \cdot m^{-1}$]
α_{SiC}	Coefficient of linear thermal expansion of SiC ceramic	[K^{-1}]
α_{Steel}	Coefficient of linear thermal expansion of steel	[K^{-1}]
L	Length	[m]
T	Temperature	[K]